



Deposited via The University of Leeds.

White Rose Research Online URL for this paper:

<https://eprints.whiterose.ac.uk/id/eprint/165503/>

Version: Accepted Version

---

**Article:**

Raveendran, R, Nagaraj, M and Namboothiry, MAG (2020) High performance, transparent solution-processed organic field effect transistor with low-k elastomeric gate dielectric and liquid crystalline semiconductor: Promises and Challenges. ACS Applied Electronic Materials. acsaelm.0c00635. ISSN: 2637-6113

<https://doi.org/10.1021/acsaelm.0c00635>

---

© 2020 American Chemical Society. This is an author produced version of an article published in ACS Applied Electronic Materials. Uploaded in accordance with the publisher's self-archiving policy.

**Reuse**

Items deposited in White Rose Research Online are protected by copyright, with all rights reserved unless indicated otherwise. They may be downloaded and/or printed for private study, or other acts as permitted by national copyright laws. The publisher or other rights holders may allow further reproduction and re-use of the full text version. This is indicated by the licence information on the White Rose Research Online record for the item.

**Takedown**

If you consider content in White Rose Research Online to be in breach of UK law, please notify us by emailing [eprints@whiterose.ac.uk](mailto:eprints@whiterose.ac.uk) including the URL of the record and the reason for the withdrawal request.

## High performance, transparent solution-processed organic field effect transistor with low-k elastomeric gate dielectric and liquid crystalline semiconductor: Promises and Challenges

Reshma Raveendran, Mamatha Nagaraj, and Manoj A G Namboothiry

*ACS Appl. Electron. Mater.*, **Just Accepted Manuscript** • DOI: 10.1021/acsaelm.0c00635 • Publication Date (Web): 13 Sep 2020

Downloaded from [pubs.acs.org](https://pubs.acs.org) on September 14, 2020

### Just Accepted

“Just Accepted” manuscripts have been peer-reviewed and accepted for publication. They are posted online prior to technical editing, formatting for publication and author proofing. The American Chemical Society provides “Just Accepted” as a service to the research community to expedite the dissemination of scientific material as soon as possible after acceptance. “Just Accepted” manuscripts appear in full in PDF format accompanied by an HTML abstract. “Just Accepted” manuscripts have been fully peer reviewed, but should not be considered the official version of record. They are citable by the Digital Object Identifier (DOI®). “Just Accepted” is an optional service offered to authors. Therefore, the “Just Accepted” Web site may not include all articles that will be published in the journal. After a manuscript is technically edited and formatted, it will be removed from the “Just Accepted” Web site and published as an ASAP article. Note that technical editing may introduce minor changes to the manuscript text and/or graphics which could affect content, and all legal disclaimers and ethical guidelines that apply to the journal pertain. ACS cannot be held responsible for errors or consequences arising from the use of information contained in these “Just Accepted” manuscripts.

1  
2  
3  
4  
5  
6  
7 **High performance, transparent solution-**  
8  
9  
10  
11 **processed organic field effect transistor with low-**  
12  
13  
14  
15 **k elastomeric gate dielectric and liquid crystalline**  
16  
17  
18  
19 **semiconductor: Promises and Challenges**  
20  
21  
22  
23

24 *Reshma Raveendran<sup>1</sup>, Mamatha Nagaraj<sup>2</sup> and Manoj A. G. Namboothiry<sup>1,\*</sup>*  
25  
26

27  
28 <sup>1</sup>School of Physics, Indian Institute of Science Education and Research- Thiruvananthapuram,  
29 Maruthamala P O, Vithura, Thiruvananthapuram, Kerala- 695551, India  
30  
31

32 E-mail: manoj@iisertvm.ac.in  
33  
34

35  
36 <sup>2</sup>School of Physics and Astronomy, University of Leeds, Leeds LS2 9JT, UK  
37

38 E-mail: m.nagaraj@leeds.ac.uk  
39  
40  
41  
42

43 **KEYWORDS:** organic field effect transistors, elastomers, polydimethylsiloxane, liquid crystals,  
44 mobility, transparent, double-slope, anomalous bias-stress  
45  
46  
47  
48

49 **ABSTRACT:** The highly flexible and stretchable polymer elastomer having a low dielectric  
50 constant ( $k \sim 2.6$ ), called poly(dimethylsiloxane) (PDMS), is a promising gate dielectric material  
51 for solution-processed organic field effect transistors (OFETs). A detailed understanding of PDMS  
52  
53  
54  
55  
56  
57  
58  
59  
60

1  
2  
3 based OFETs is required to extend its application to flexible electronic devices. The present work  
4 discusses about the promises and challenges of PDMS based solution-processed OFETs using a  
5 liquid crystal (LC), 2-decyl-7-phenyl-benzothienobenzothiophene (Ph-BTBT-10) as  
6 semiconducting channel material. The liquid crystal-OFET (LC-OFET) exhibits high electrical  
7 performance such as high hole mobility of  $\sim 22 \text{ cm}^2\text{V}^{-1}\text{s}^{-1}$ , low threshold voltage ( $< 1 \text{ V}$ ) and high  
8 current on/ off ratio of  $10^5$ . The OFETs also show high optical transparency ( $> 90 \%$ ). The  
9 electrical performance of LC-OFETs are observed to have a significant correlation with the  
10 annealing temperature of Ph-BTBT-10 layer and is also influenced by the different operating  
11 conditions such as air, nitrogen and vacuum. The OFETs demonstrate anomalous bias stress  
12 behavior and hysteresis which are also addressed.  
13  
14  
15  
16  
17  
18  
19  
20  
21  
22  
23  
24  
25  
26

## 27 INTRODUCTION

28  
29  
30  
31 Organic field effect transistor (OFET), a vital key component in organic electronic circuits, is  
32 actively investigated during the last thirty years and tremendous progress has been made in its  
33 performance. OFETs have the potential to enable large area, flexible electronic circuitry at a low-  
34 cost of production and find application in radio frequency identification (RFID) tags, smart cards,  
35 electronic papers and active matrix displays.<sup>1</sup> Moreover, OFETs with high optical transparency  
36 and environmental stability are potentially suitable for next generation transparent electronics such  
37 as flat panel displays and sensor arrays.<sup>2-5</sup> The unique features of mechanical flexibility, tunability  
38 of electrical and optical properties and solution-processability enjoyed by OFETs are realized by  
39 the organic components used in them, namely the organic semiconductor (OSC), the gate dielectric  
40 and the electrodes.<sup>6-8</sup>  
41  
42  
43  
44  
45  
46  
47  
48  
49  
50  
51  
52  
53  
54  
55  
56  
57  
58  
59  
60

1  
2  
3 Gate dielectric plays a crucial role in determining the characteristics of an OFET as the channel  
4 is just a few monolayers above the dielectric.<sup>7, 9-12</sup> In most of the high-performance OFETs reported  
5 so far, the conventional inorganic materials such as silicon dioxide (SiO<sub>2</sub>), aluminum oxide (Al<sub>2</sub>O<sub>3</sub>)  
6 and so on are used as gate dielectrics along with solution-processed OSCs.<sup>13-20</sup> Though, all-  
7 solution-processed OFETs are essential for the realization of low-cost, flexible electronic devices,  
8 the development of such OFETs in which both the gate dielectric and the semiconductor are  
9 organic materials is difficult to achieve. The reason being the difficulty in forming pin-hole free  
10 dielectric thin-films with controlled morphology and selection of suitable orthogonal solvent for  
11 both the semiconductor and the gate dielectric.<sup>12</sup> However, there is a large improvement in the  
12 development of flexible gate dielectrics these days.<sup>8, 21-25</sup> To ensure good electrical performance,  
13 dielectrics of high dielectric constant (high-k) are often suggested.<sup>26</sup> However, as high-k materials  
14 suffer from large dipole disorder, high gate leakage current, large power dissipation and low  
15 reproducibility, low-k dielectrics can be considered to make more reliable low-power devices.<sup>7-8,</sup>  
16  
17  
18  
19  
20  
21  
22  
23  
24  
25  
26  
27  
28  
29  
30  
31  
32  
33  
34  
35  
36  
37  
38  
39  
40  
41  
42  
43  
44  
45  
46  
47  
48  
49  
50  
51  
52  
53  
54  
55  
56  
57  
58  
59  
60

10, 21, 27-29 Among the various low-k dielectrics, the polymer elastomer, polydimethylsiloxane (PDMS), is a promising candidate as a gate dielectric in OFETs as it exhibits high flexibility, stretchability and good optical transparency.<sup>30-33</sup> However, it has mainly been used along with vacuum-deposited semiconductors, as solution-processing on PDMS surface is difficult due to its high hydrophobic nature and low surface energy.<sup>33-35</sup> The applicability of PDMS in OFETs is critically limited by these aspects and hence it is less explored. Our recent work has shown that the wettability and adhesion of organic solutions on PDMS can be accomplished by mere treatment of PDMS surface with ultra-violet ozone (UVO) for an extended period of time. Our findings demonstrated the possibility of using PDMS as a gate dielectric in all-solution-processed OFETs.<sup>36</sup>

1  
2  
3 The applicability of OFETs in electronic circuits is assessed by its current on-off ratio and  
4 switching frequency.<sup>37</sup> Since both these parameters are highly dependent on charge carrier  
5 mobility, it remains a crucial figure of merit of OFETs.<sup>37-38</sup> Significant efforts have been devoted  
6 to realize high mobility OSCs which form the channel for carrier conduction in FETs. OFETs  
7 fabricated with solution-processed OSCs are reported to show field effect mobilities above 10  
8  $\text{cm}^2\text{V}^{-1}\text{s}^{-1}$ .<sup>2, 13-20, 39</sup> Crystallinity and uniformity of the semiconducting films critically affect the  
9 mobility. In most of the solution-processed films, poor uniformity and high roughness occur due  
10 to recrystallization of the materials during solvent evaporation.<sup>9</sup> In this perspective, there is much  
11 focus on the utilization of solution-processable semiconducting liquid crystals (LCs) that form  
12 high-quality dielectric-semiconductor interfaces by enhanced crystalline ordering and self-  
13 alignment, thereby improving the charge carrier transport through the channel.<sup>13, 40-41</sup> Besides this,  
14 the temperature stability of LCs from ambient to 100-200 °C promises viable practical  
15 applications.<sup>41</sup> In this work, we address these issues and report OFETs of high mobilities,  
16 fabricated on flexible polymer elastomer called PDMS.

17  
18  
19 Recently, Iino and coworkers developed a LC semiconducting material namely, 2-decyl-7-  
20 phenyl-benzothienobenzothiophene (Ph- BTBT-10) which shows two LC mesophases, smectic E  
21 (SmE) and smectic A (SmA). They demonstrated the application of Ph-BTBT-10 as channel  
22 material in OFETs with the conventional gate dielectric, silicon dioxide ( $\text{SiO}_2$ ) and the OFETs  
23 exhibited a mobility value of  $13.9 \text{ cm}^2\text{V}^{-1}\text{s}^{-1}$ .<sup>9</sup> The high mobility is attributed to the closely packed  
24 crystal-like molecular ordering (called herringbone structure) of Ph-BTBT-10 in its SmE phase  
25 which allows two-dimensional conduction.<sup>9</sup> The same group has investigated the characteristics  
26 of Ph-BTBT-10 based OFET with a hybrid gate insulator, polystyrene (PS)/  $\text{SiO}_2$  and obtained a  
27 low average threshold voltage ( $V_{\text{th}}$ ) of  $-0.12 \pm 0.09 \text{ V}$ , compromising the mobility ( $\mu_{\text{sat}} = 3.8 \pm$   
28  
29  
30  
31  
32  
33  
34  
35  
36  
37  
38  
39  
40  
41  
42  
43  
44  
45  
46  
47  
48  
49  
50  
51  
52  
53  
54  
55  
56  
57  
58  
59  
60

1  
2  
3 0.27  $\text{cm}^2\text{V}^{-1}\text{s}^{-1}$ ) and flexibility.<sup>10</sup> Later, Kim et al. studied the effect of semiconductor annealing  
4 temperatures on the performance of OFETs fabricated with polyimide (PI)/ alumina ( $\text{Al}_2\text{O}_3$ ) gate  
5 dielectric. They obtained a maximum mobility of  $2.27 \text{ cm}^2\text{V}^{-1}\text{s}^{-1}$  with Ph-BTBT-10 layer annealed  
6 at  $140^\circ\text{C}$  (temperature corresponds to the SmE phase) but the devices operated at a high  $V_{\text{th}}$  of  $\sim$   
7 - 12 V.<sup>11</sup> In all these reports, either a conventional gate dielectric ( $\text{SiO}_2$ ) or a bilayer of organic and  
8 conventional gate dielectric (PS/  $\text{SiO}_2$  and PI/  $\text{Al}_2\text{O}_3$ ) are used. Implementation of elastomeric gate  
9 dielectrics in LC-OFETs is less reported in the literature and since each dielectric-semiconductor  
10 interface has its unique features, it would be interesting to investigate how an elastomeric gate  
11 dielectric such as PDMS influences the performance of LC-OFETs. Being a well-known material  
12 for its high flexibility and stretchability, the incorporation of PDMS in OFETs may have a future  
13 implication in the development of flexible electronic devices.

14  
15  
16  
17  
18  
19  
20  
21  
22  
23  
24  
25  
26  
27  
28  
29  
30 In the present work, the performance of solution-processed OFETs with Ph-BTBT-10 as  
31 semiconductor and PDMS as gate dielectric is discussed. Two sets of OFETs have been fabricated  
32 for the studies, one set is made in ambient air and the other set is fabricated in inert condition (in  
33 nitrogen atmosphere). Surface treated PDMS layer (extended ultra violet-ozone (UVO) treatment  
34 for 60 minutes) is used in the study. A detailed description of UVO treatment and its consequences  
35 are described in our previous work.<sup>36</sup> A systematic study on the effect of different annealing  
36 temperatures of Ph-BTBT-10 layer on the performance of OFETs is conducted and the effect of  
37 different environmental conditions is evaluated. Deviation from ideal transistor behavior is  
38 observed in the OFETs in the form of double slopes which can cause overestimation of the mobility  
39 values.<sup>42</sup> This issue has been addressed and the reliability of extracted mobilities is inspected by  
40 calculating 'reliability factor ( $r$ )' as recently reported by H. H. Choi et al.<sup>42</sup> Accordingly, the OFET  
41 with Ph-BTBT-10 layer annealed at  $120^\circ\text{C}$  in air exhibited the highest mobility of  $\sim 22.7 \text{ cm}^2 \text{ V}^{-1}$

1  
2  
3  $s^{-1}$ , low threshold voltage (+ 0.76 V) and high current on/ off ratio ( $10^5$ ) compared to other OFETs.  
4  
5 The LC-OFET also exhibited good transparency (> 90%) owing to the transparent nature of the  
6  
7 components, indium tin oxide (ITO) gate electrode, PDMS and Ph-BTBT-10 used in the device  
8  
9 architecture. The correlation between the outstanding performance of OFETs with the change in  
10  
11 morphology and crystallinity of Ph-BTBT-10 with annealing temperature is investigated. The  
12  
13 crystalline and morphological features of annealed films of Ph-BTBT-10 are studied by means of  
14  
15 small angle x-ray scattering (SAXS), x-ray diffraction (XRD) and atomic force microscopy (AFM)  
16  
17 techniques. The electrical stability of OFETs is analyzed by conducting bias-stress measurements  
18  
19 and the environmental stability is analyzed by evaluating the OFET performance in air, nitrogen  
20  
21 and vacuum conditions. Hysteresis is observed in the PDMS based LC-OFETs which is also  
22  
23 discussed in detail.  
24  
25  
26  
27  
28

## 29 **EXPERIMENTAL SECTION**

30  
31  
32  
33 **Materials.** Commercially available Ph-BTBT-10 (MW= 456.706 g/mol) from TCI Chemicals and  
34  
35 PDMS along with its curing agent (Sylgard 184) from Dow corning were used as the  
36  
37 semiconductor and gate dielectric respectively. ITO substrates were purchased from ( $10 \Omega/\text{cm}^2$ )  
38  
39 Delta Technologies Inc., USA.  
40  
41

42  
43 **LC-OFET fabrication.** The OFETs were fabricated in the bottom-gate top-contact (BGTC)  
44  
45 configuration (figure 1a) on ITO coated glass substrates. The gate dielectric, PDMS and the  
46  
47 semiconductor, Ph-BTBT-10 (chemical structures as shown in figure 1b) were solution-processed  
48  
49 using spin-coating method. PDMS was mixed thoroughly with a curing agent at 10:1 w/w ratio to  
50  
51 initiate cross-linking and mixed with cyclohexane (PDMS/ cyclohexane= 1:6 w/w ratio) to reduce  
52  
53 the viscosity of the solution. Thin-films of PDMS was prepared by spin-coating PDMS solution at  
54  
55  
56  
57  
58  
59  
60

1  
2  
3 an rpm of 6000 on ITO substrate and annealed the layer at 150 °C for 30 minutes. These films with  
4  
5 thickness around 1.2 μm (measured using Alpha-Step D-600 Stylus Profiler, KLA Tencor) were  
6  
7 UVO treated for 60 minutes in a UV-Ozone cleaner with an output power of 9 mW/cm<sup>2</sup> (UVOCS,  
8  
9 USA) to enhance the surface wettability of PDMS (more details on the UVO treatment of PDMS  
10  
11 surface is provided in the supporting information). Thin- films of Ph-BTBT-10 was spin-coated  
12  
13 from a solution prepared by dissolving it in chlorobenzene (CB) (0.66 wt %). Prior to spin-coating,  
14  
15 the solution was stirred by heating it at 160 °C for 5 minutes and kept for continuous stirring at  
16  
17 110 °C to ensure complete dissolution. At this temperature, the LC exists in one of its mesophases  
18  
19 called, the SmE phase (details of the polarization optical microscopy (POM) and differential  
20  
21 scanning calorimetry (DSC) studies of the LC are given in the supplementary data, figure S1). The  
22  
23 solution was immediately spin-coated on PDMS surface to avoid sudden crystallization into bulk  
24  
25 layers. The layers were annealed at different temperatures (120 °C, 180 °C and 218 °C) for 10  
26  
27 minutes each. The Ph-BTBT-10 film thickness was measured to be ~ 35 nm. The source and drain  
28  
29 electrodes were deposited by the thermal evaporation of gold (Au) using a mask with channel  
30  
31 length, L= 30 μm and channel width, W= 1 mm.  
32  
33  
34  
35  
36  
37

38 ***LC-OFET characterization.*** The OFETs were characterized using Keithley SCS 4200 Parameter  
39  
40 analyzer and the mobility in the saturation regime ( $\mu_{sat}$ ) was calculated using the following  
41  
42 equation,  
43  
44  
45

$$\mu_{sat} = \frac{2L}{W C_i} \left( \frac{\partial \sqrt{I_{DS}}}{\partial V_{GS}} \right)^2 \quad (1)$$

46  
47  
48  
49  
50 Where  $C_i$  is the capacitance per unit area of the gate dielectric,  $W$  is the channel width and  $L$  is  
51  
52 the channel length. The capacitance characterization of PDMS is conducted using Agilent E4980A  
53  
54 Precision LCR Meter.  
55  
56  
57  
58  
59  
60

1  
2  
3 The reliability of the extracted mobilities are examined by calculating ‘reliability factor (r)’ as  
4 suggested by Choi *et al.*, using the equation given below.  
5  
6

7  
8 The reliability factor (r) in the saturation regime:<sup>42</sup>  
9

$$r_{sat} = \left( \frac{\sqrt{|I_{DS}|_{max}} - \sqrt{|I_{DS}|_0}}{|V_{GS}|_{max}} \right)^2 / \left( \frac{\partial \sqrt{|I_{DS}|}}{\partial V_{GS}} \right)^2_{claimed} \quad (2)$$

10  
11  
12 where,  $|I_{DS}|_{max}$  is the maximum saturation drain current for the maximum gate to source voltage  
13 ( $|V_{GS}|_{max}$ ),  $|I_{DS}|_0$  is the drain current at zero  $V_{GS}$ ,  $\mu_{claimed}$  is the claimed mobility obtained directly  
14 from the Shockley equation (1). The experiments were conducted in air, nitrogen and vacuum  
15 conditions.  
16  
17  
18  
19  
20  
21  
22  
23  
24

25 **Characterization of Ph-BTBT-10.** To study the characteristics of Ph-BTBT-10, the polarization  
26 optical microscopy (POM) images were taken using Leica DM2700P polarization microscope.  
27  
28 The sample was mounted on a Linkam THMS600 hot stage and the temperature was controlled  
29 using Linkam T95-PE temperature controller (cooling rate 0.1 °C/min). Differential scanning  
30 calorimetry (DSC) measurements were done using DSC Q20, TA Instruments. Small angle X-ray  
31 scattering (SAXS) was done using Xeuss SAXS/WAXS system, Xenocs. The crystalline  
32 properties and morphology of the LC films on glass substrate and on PDMS surface were studied  
33 using X-ray diffraction (PANalytical Empyrean XRD) and atomic force microscopy (Nanowizard  
34 4 AFM, JPK Instruments) techniques respectively. The transparency of Ph-BTBT-10 films were  
35 evaluated using an ultraviolet-visible spectroscopic technique (LAMBDA 950 UV/Vis  
36 Spectrophotometer, PerkinElmer). Bias- stress measurements were conducted by using two source  
37 meters from Keithley (6430 and 2400).  
38  
39  
40  
41  
42  
43  
44  
45  
46  
47  
48  
49  
50  
51  
52  
53  
54  
55  
56  
57  
58  
59  
60

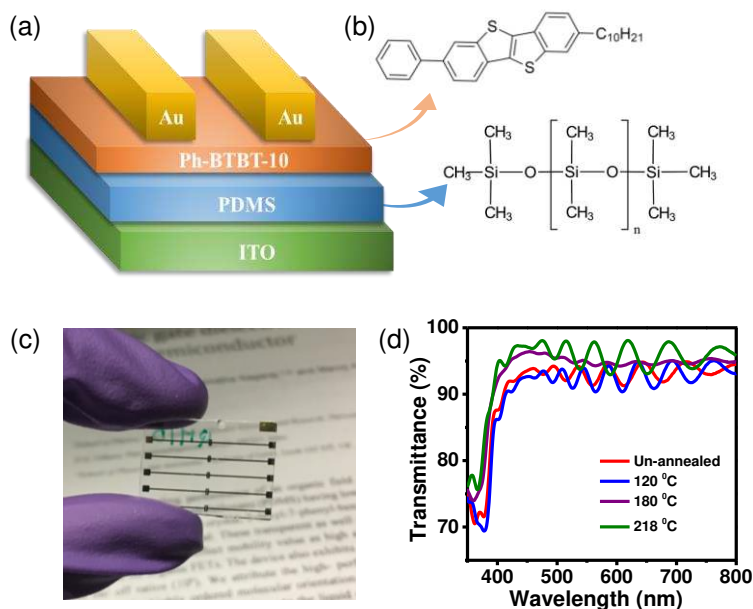


**Figure 1.** (a) Schematic representation of the device architecture of a bottom-gate top-contact OFET. (b) Molecular structure of the liquid crystal, Ph-BTBT-10 (top) and the polymer, PDMS (bottom). (c) Photograph showing a prepared transparent OFET and (d) UV-Visible transmission spectra of ITO/ PDMS/ Ph-BTBT-10 film structure at different annealing temperatures of Ph-BTBT-10.

## RESULTS AND DISCUSSION

**Transistor Characteristics at different annealing temperatures of Ph-BTBT-10.** The solution-processed OFETs are fabricated in the bottom-gate top-contact (BGTC) configuration using PDMS as gate dielectric and Ph-BTBT-10 as semiconductor material (Figure 1a, 1b). Solution-processing of Ph-BTBT-10 is enabled on PDMS surface by extended ultra violet-ozone (UVO) treatment as discussed in our previous work.<sup>36</sup> The UVO working mechanism is included in the supporting information. The gate dielectric PDMS of thickness around 1.2  $\mu\text{m}$  exhibits a capacitance per unit area ( $C_i$ ) of  $\sim 1.92 \text{ nF cm}^{-2}$  at frequency,  $f = 1 \text{ kHz}$ . The capacitance-frequency

1  
2  
3 plot of PDMS (figure S2) shows almost a constant value of capacitance for a long range of  
4  
5 frequency (100 Hz to 2 MHz). The semiconductor, Ph-BTBT-10 formed uniform thin layer of  
6  
7 thickness  $\sim 35$  nm which is annealed at different temperatures, 120  $^{\circ}\text{C}$ , 180  $^{\circ}\text{C}$  and 218  $^{\circ}\text{C}$ , to  
8  
9 analyze its effect on the electrical performance of LC-OFETs. The temperatures were chosen in  
10  
11 such a way that the LC exists in the SmE phase (at 120 and 180  $^{\circ}\text{C}$ ) and in the SmA phase (at 218  
12  
13  $^{\circ}\text{C}$ ) during annealing (figure S1). Figure 1c shows the photograph of the prepared LC-OFET. The  
14  
15 OFETs at all annealing temperatures exhibit high optical transparency  $> 90\%$  in the visible region  
16  
17 as shown in the UV-vis transmission spectra (figure 1d). More than twenty devices have been  
18  
19 fabricated at each annealing temperatures by keeping other processing conditions the same and the  
20  
21 best characteristics obtained are shown in figure 2. The devices exhibited small gate leakage  
22  
23 currents which are 2-3 orders lower than the drain current as seen in figure 2(b,d,f and h). The  
24  
25 output characteristics of all the devices showed distinct linear and saturation regimes with drain  
26  
27 current ( $I_{\text{DS}}$ ) in the mA range for different applied gate voltages ( $V_{\text{GS}}$ ). However, the output  
28  
29 characteristics exhibited non-linear behavior at low drain to source voltage ( $V_{\text{DS}}$ ) which indicates  
30  
31 the presence of substantial contact resistance.<sup>43,44</sup> The main source of contact resistance is the  
32  
33 misalignment between the work function of gold electrode (- 5.1 eV) and the highest occupied  
34  
35 molecular orbital (HOMO) energy level of Ph-BTBT-10 (- 5.6 eV).<sup>43, 45</sup> A non-ideal behavior is  
36  
37 observed in the transfer characteristics of OFETs in the form of double slopes (or kinks) where the  
38  
39 Ph-BTBT-10 film is either un-annealed or annealed at 120  $^{\circ}\text{C}$  (figure 2b and 2d). Kink in the  
40  
41 transfer characteristics are often caused by contact effects in OFETs.<sup>44, 46</sup> Here, the appearance of  
42  
43 kinks in OFETs with the semiconductor film annealed at certain specific temperatures indicates its  
44  
45 correlation with the changes occurring in the microstructure of the film or at the semiconductor-  
46  
47 dielectric interface. As it is seen in the figures 2b and 2d, there are two slopes in the transfer curve  
48  
49  
50  
51  
52  
53  
54  
55  
56  
57  
58  
59  
60

1  
2  
3 (a high slope region at low  $V_{GS}$  and a small slope region at high  $V_{GS}$ ). Therefore, the conventional  
4 way of calculation can lead to wrong estimation of mobilities.<sup>42, 44</sup> Being a common issue among  
5 high mobility OFETs,<sup>2, 47</sup> it is often suggested to estimate the mobility from low slope (high  $V_{GS}$ )  
6 region of the transfer curve in order to get more accurate value.<sup>42, 44, 48</sup> We have calculated  
7 mobilities using both the slopes and analyzed the closeness of the derived mobilities (for the  
8 OFETs with double-slope) to an equivalent OFET with the same maximum saturation current ( $I_{D}$   
9  $_{sat}$ ) at a maximum gate voltage ( $V_{GS}$ ) using reliability factor ( $r$ ) calculation (equation 2 in the  
10 experimental section) which is recently suggested by H. H. Choi et al (summarized in table S1).<sup>42</sup>  
11 The mobilities derived from the high slope region of OFETs with Ph-BTBT-10 film un-annealed  
12 and annealed at 120 °C are found to have low reliability factors (43 and 34 % respectively)  
13 compared to that of the equivalent ideal OFET. Whereas, the mobilities derived from the small  
14 slope region are found to be closer to the mobility of equivalent OFETs with reliability factors 92  
15 and 91 % respectively. Hence, we choose the mobility derived from the small slope region as the  
16 original hole mobility for those devices which show the abnormal 'kinks'. The threshold voltages  
17  $V_{th}$  are also obtained by considering the small slope in the  $\sqrt{I_{DS}}$  vs  $V_{GS}$  curve. The mobility of the  
18 devices annealed at 180 and 218 °C are obtained using the conventional method. Linear mobility  
19 of the OFETs are not included in the table as they are prone to contact effects. The electrical  
20 parameters obtained for the OFETs shown in figure 2 are as given in table 1. The average mobilities  
21 of ten to fifteen OFETs for each annealing temperatures are tabulated (table S2) and the variation  
22 in mobility with different annealing temperatures of Ph-BTBT-10 are shown in figure S3 (the  
23 figure also shows the mobility values of the devices annealed at intermediate temperatures of 100  
24 and 150 °C with error bars included) where sudden jump in mobility at 120 °C is clearly visible.  
25  
26 A similar trend is observed in the case of threshold voltages and current on/ off ratios also. It is to  
27  
28  
29  
30  
31  
32  
33  
34  
35  
36  
37  
38  
39  
40  
41  
42  
43  
44  
45  
46  
47  
48  
49  
50  
51  
52  
53  
54  
55  
56  
57  
58  
59  
60

1  
2  
3 be noted that some of the OFETs showed mobilities higher than the highest value reported here,  
4  
5 but were not reproducible and therefore avoided.  
6  
7

8  
9 It is seen that the transistor characteristics show significant dependence on the annealing  
10 temperatures (un-annealed, annealed at 120 °C, 180 °C and 218 °C) of Ph-BTBT-10 film. Among  
11 them, the OFET with LC film annealed at 120 °C exhibited considerably higher drain currents,  
12 high mobility, low threshold voltage and high current on-off ratio compared to other OFETs. The  
13 hole- mobility of the OFET with un-annealed Ph-BTBT-10 layer is obtained as  $5.56 \text{ cm}^2 \text{ V}^{-1} \text{ s}^{-1}$   
14 and possessed a low  $V_{\text{th}}$  of  $-0.87 \text{ V}$ , when calculated from the low-slope (high  $V_{\text{GS}}$  region). As  
15 the annealing temperature is increased to 120 °C, the mobility increased almost four times to  $22.71$   
16  $\text{cm}^2 \text{ V}^{-1} \text{ s}^{-1}$ , which is to the best of our knowledge, the highest mobility value reported for Ph-  
17 BTBT-10 based OFET. The mobility averaged for twenty devices are obtained as  $22 \pm 2 \text{ cm}^2 \text{ V}^{-1}$   
18  $\text{s}^{-1}$ . The device is operated at a very low, close to zero  $V_{\text{th}}$  of  $+0.76 \text{ V}$  and exhibited high current  
19 on/ off ratio of  $\sim 10^5$ . However, for the OFET with Ph-BTBT-10 layer annealed at 180 °C, the  
20 mobility fall down to  $3.41 \text{ cm}^2 \text{ V}^{-1} \text{ s}^{-1}$  and the  $V_{\text{th}}$  is increased to  $-12.06 \text{ V}$ . On further increasing  
21 the annealing temperature to 218 °C, a sudden drop in mobility to  $0.5 \text{ cm}^2 \text{ V}^{-1} \text{ s}^{-1}$  along with a rise  
22 in  $V_{\text{th}}$  is observed.  
23  
24  
25  
26  
27  
28  
29  
30  
31  
32  
33  
34  
35  
36  
37  
38  
39  
40  
41  
42  
43  
44  
45  
46  
47  
48  
49  
50  
51  
52  
53  
54  
55  
56  
57  
58  
59  
60

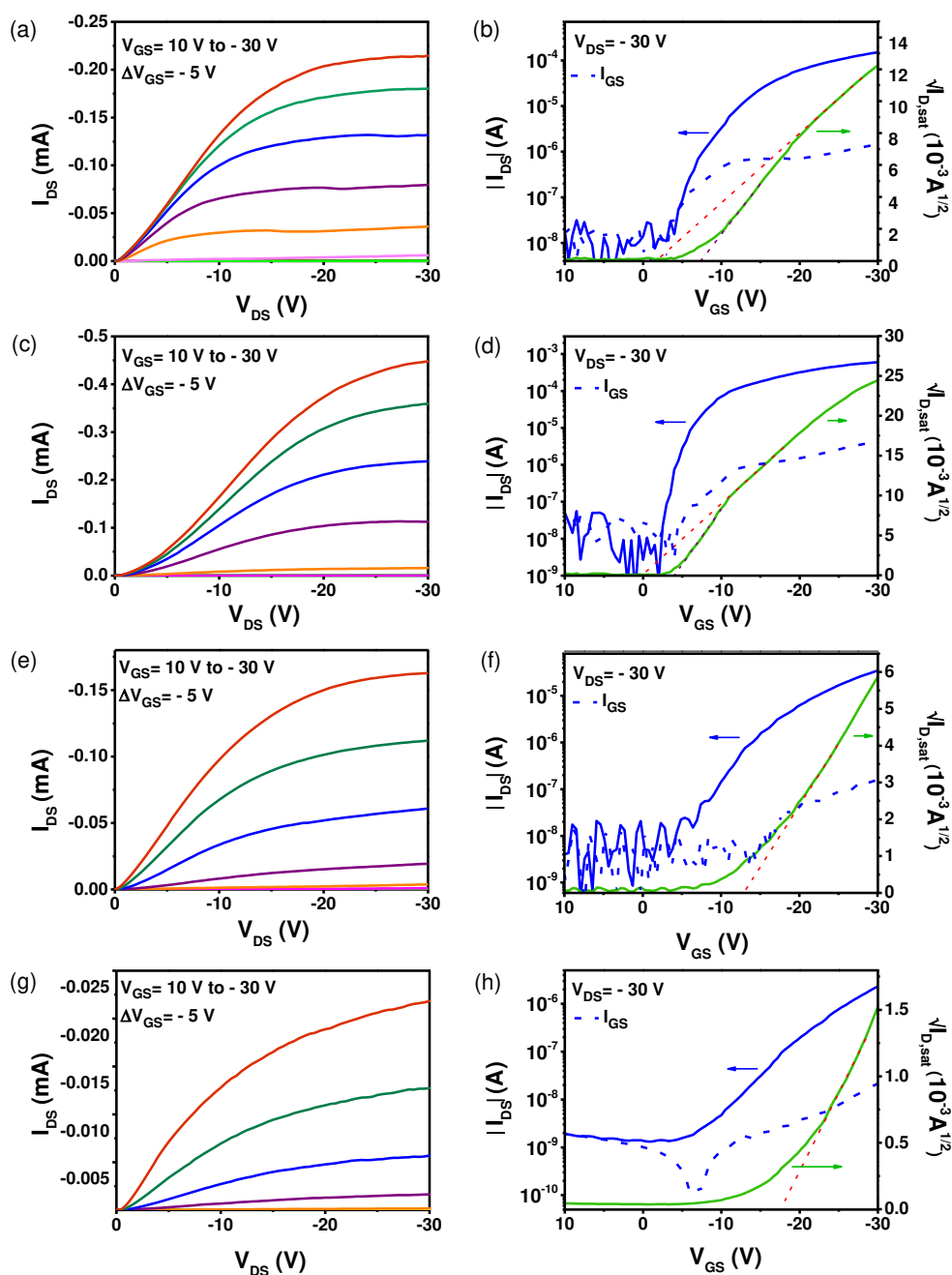


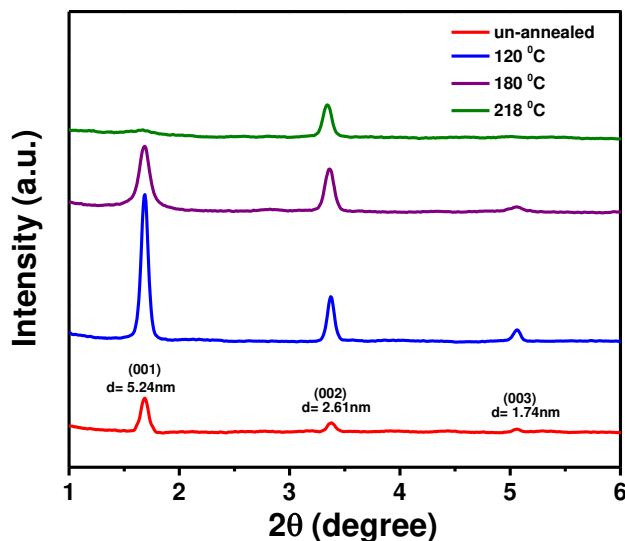
**Figure 2.** (a, c, e, g) Output characteristics ( $I_{DS}$  -  $V_{DS}$ ) and (b, d, f, h) transfer characteristics ( $|I_{DS}|$  -  $V_{GS}$  and  $\sqrt{|I_{D,sat}|}$  -  $V_{GS}$ ) at  $V_{DS} = -30$  V of OFETs at annealing temperatures (a, b) un-annealed (c, d) 120 °C (e, f) 180 °C (g, h) 218 °C. The dashed blue line in (b, d, f and h) represents gate leakage current in the OFETs.

**Table 1.** Electrical parameters of obtained for the LC-OFETs shown in figure 2 at different annealing temperatures of Ph-BTBT-10.

Annealing temperature (°C)	Saturation Mobility, $\mu_{\text{sat}}$ ( $\text{cm}^2 \text{V}^{-1} \text{s}^{-1}$ )	$V_{\text{th}}$ (V)	$I_{\text{On}}/ I_{\text{Off}}$
Un-annealed	5.56	- 0.87	$2 \times 10^4$
120	22.71	+ 0.76	$6 \times 10^5$
180	3.41	- 16.08	$7 \times 10^3$
218	0.5	- 18.20	$1 \times 10^3$

**Ph-BTBT-10 Layer Characterization.** The electrical characteristics of OFETs show clear dependence on the annealing temperatures of Ph-BTBT-10. Here, we rule out the influence of underlying PDMS layer as the cross-linked PDMS is stable up to  $\sim 200$  °C.<sup>49</sup> To investigate it in detail, a systematic study of the structural and morphological properties of thermally annealed Ph-BTBT-10 was carried out using small angle x-ray scattering (SAXS), x-ray diffraction (XRD) and atomic force microscopy (AFM) techniques. All these experiments were conducted by annealing Ph-BTBT-10 at room temperature, which are either in their thin/ bulk-film form or in powder form according to the requirement of the technique. To conduct SAXS measurement, the Ph-BTBT-10 films were initially coated on glass substrate and annealed at temperatures 120, 180 and 218 °C. The material is then scratched out of the glass into powder form after cooling it down to room temperature. Figure 3 shows the SAXS pattern obtained for Ph-BTBT-10 at different processing temperatures. A comparatively high intensity peak (001), which corresponds to a d-spacing of 5.24 nm, is observed for the samples that are un-annealed, annealed at 120 and 180 °C. This peak represents the typical bilayer structure of the SmE phase of Ph-BTBT-10.<sup>11, 50</sup> Whereas, for the

1  
2  
3 sample annealed at 218 °C (temperature corresponding to the SmA phase), only a single peak  
4 corresponding to the (002) plane is present. This peak corresponds to a d-spacing of 2.61nm, which  
5  
6  
7 is the length of one Ph-BTBT-10 molecule, and so the material has a monolayer structure.<sup>9, 11, 50-51</sup>  
8  
9  
10 Hence, it can be concluded that the Ph-BTBT-10 structure has undergone a complete transition  
11  
12 from bilayer to monolayer as the temperature is increased above its SmE to SmA phase transition  
13  
14 temperature (~ 211 °C as per the DSC curve shown in figure S1).<sup>9, 11</sup> Interestingly, even after  
15  
16 cooling the sample down to room temperature, the annealed films continued to maintain the  
17  
18 structural properties of the SmA and SmE LC phases without undergoing any further reorientation.  
19  
20 Furthermore, the sample annealed at 120 °C exhibits a high intensity peak corresponding to the  
21  
22 (001) plane showing the presence of a bilayer structure. This indicates a strong herringbone  
23  
24 packing in it compared to other films.<sup>52</sup> These structural changes in Ph-BTBT-10 as a result of  
25  
26 thermal annealing might have affected the electrical performance OFETs as the charge carrier  
27  
28 transport occurs through the semiconductor channel.  
29  
30  
31  
32  
33



54 **Figure 3.** SAXS pattern of Ph-BTBT-10 powder annealed at 120, 180 and 218 °C.  
55  
56  
57  
58  
59  
60

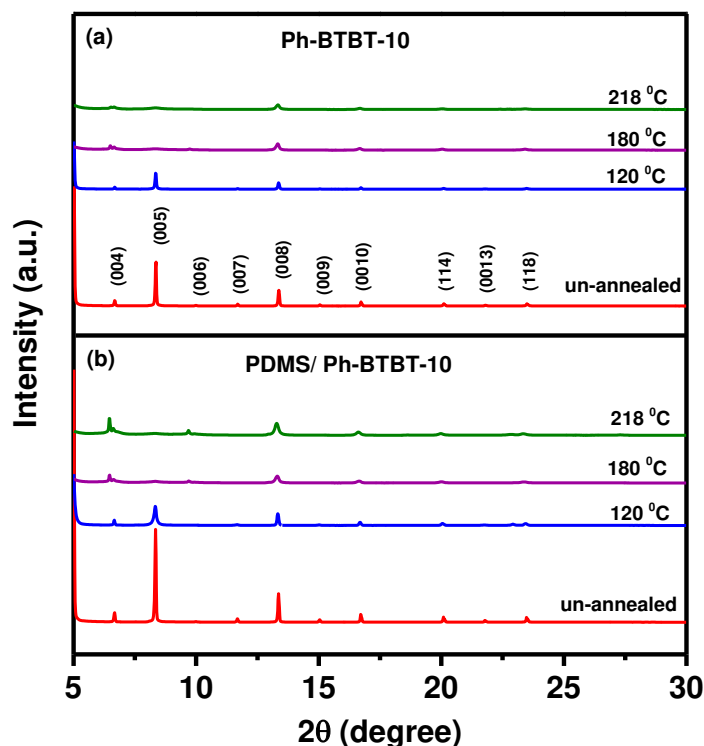


**Figure 4.** XRD pattern of Ph-BTBT-10 films drop-casted on (a) glass surface and (b) PDMS surface that are annealed at temperatures 120, 180 and 218 °C.

The XRD patterns of Ph-BTBT-10 films, drop-casted on glass as well as PDMS are shown in figure 4. The patterns agree with the literature values.<sup>53</sup> The XRD patterns of Ph-BTBT-10 do not show any difference with the change in substrates as seen in figure 4a and 4b. However, the intensity of the peaks seem to increase when coated on PDMS. Noticeable differences are observed among the films annealed at different temperatures. The film annealed at 120 °C and the un-annealed film have similar patterns. However, as the annealing temperature is increased, some of the peaks started disappearing or diminishing as seen in the case of films annealed at 180 and 218

<sup>0</sup>C. Here again, similar to the SAXS pattern, the XRD peaks of films annealed at 120 <sup>0</sup>C show the features of strong crystallinity compared to films annealed at higher temperatures. For example, for the un-annealed film and the film annealed at 120 <sup>0</sup>C, peak corresponding to the (005) plane is prominent whereas, at elevated temperatures these peaks become less prominent.

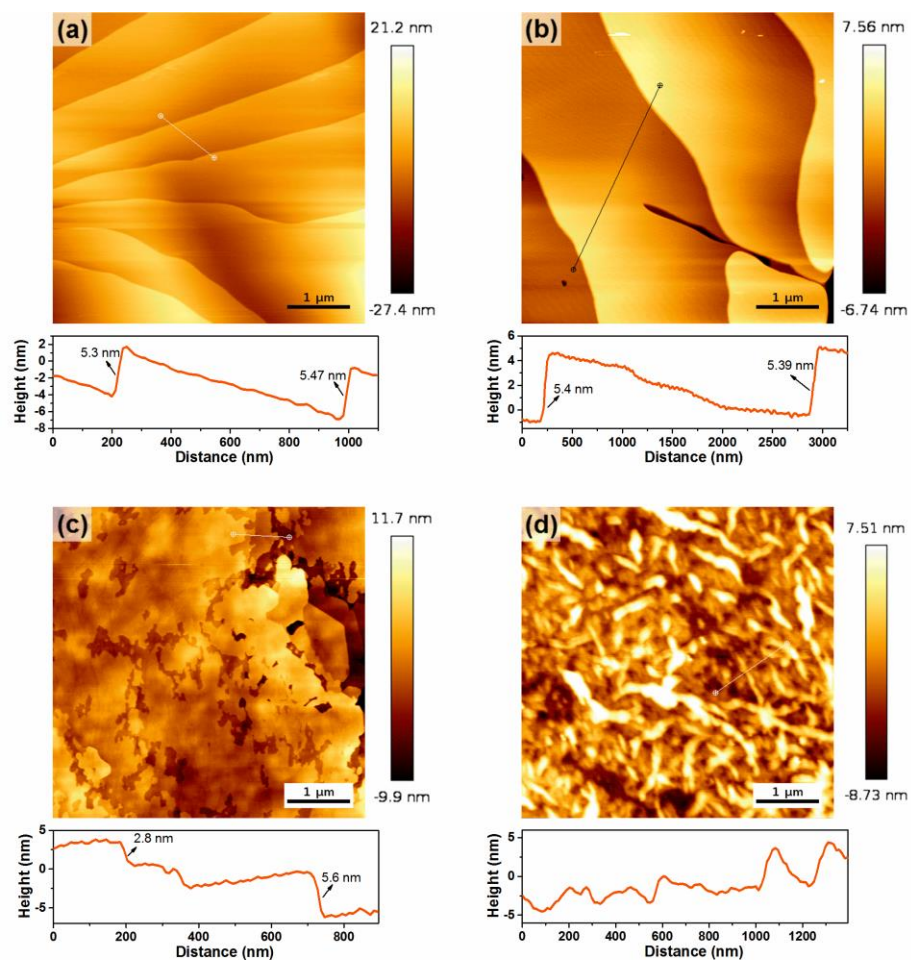


**Figure 5.** AFM images of spin-coated Ph-BTBT-10 thin films on glass surface at different annealing conditions and their corresponding surface profiles: (a) Un-annealed, annealed at (b) 120 <sup>0</sup>C, (c) 180 <sup>0</sup>C and (d) 218 <sup>0</sup>C.

1  
2  
3 Figure 5 shows the AFM images ( $5\ \mu\text{m} \times 5\ \mu\text{m}$ ) of Ph- BTBT-10 thin films spin-coated on  
4 glass surface and annealed at different temperatures. The films exhibit good material coverage  
5 over the substrate surface and possess low surface roughness (Table S3). The un-annealed film  
6 contains many well-oriented crystallites with a flake-like structure (figure 5a). A similar flat,  
7 terrace-like morphology is observed for the films annealed at  $120\ ^\circ\text{C}$  also, but here the grain size  
8 is larger (figure 5b) compared to the un-annealed film. From the surface profiling of AFM images  
9 of un-annealed films and films annealed at  $120\ ^\circ\text{C}$ , over a selected region, it is found that the height  
10 of each layer is around  $5.6\ \text{nm}$  or a multiple of it. This is an indication of the presence of bilayer  
11 structure in the films, in accordance with the results obtained from the SAXS pattern. However,  
12 as the annealing temperature is increased to  $180\ ^\circ\text{C}$ , the grain size is decreased and the film  
13 uniformity is lost (figure 5c). Also a random orientation of grains is observed. The films show  
14 regions with layer heights of  $\sim 2.8\ \text{nm}$  and  $\sim 5.6\ \text{nm}$ , which is a clear indication of the presence of  
15 both monolayer and bilayer structures.<sup>9</sup> This is again consistent with the SAXS data where the  
16 films annealed at  $180\ ^\circ\text{C}$  showed peaks of similar intensity corresponding to the d-spacing of  $2.61$   
17 nm and  $5.24\ \text{nm}$ . Whereas, when the annealing temperature is raised to  $218\ ^\circ\text{C}$ , the film  
18 morphology has changed completely and the terrace-like regions are absent in the film. The  
19 morphology of the Ph- BTBT-10 thin films on PDMS surface (see supporting information for  
20 AFM images (figure S4) and roughness data (Table S4)) is also examined. The results are similar  
21 to that obtained on glass substrates, except for the presence of smaller grains with increased surface  
22 roughness. The increased surface roughness can be associated with the wrinkled morphological  
23 features present on the UVO treated PDMS.<sup>36</sup> Wrinkles (surface with hills and valleys) generally  
24 form on the surface of the highly viscoelastic PDMS films when it is subjected to thermal curing  
25 like annealing or UVO treatment due to the release of mechanical stress.<sup>31, 36</sup> The surface roughness  
26  
27  
28  
29  
30  
31  
32  
33  
34  
35  
36  
37  
38  
39  
40  
41  
42  
43  
44  
45  
46  
47  
48  
49  
50  
51  
52  
53  
54  
55  
56  
57  
58  
59  
60

1  
2  
3 can also be caused by the evaporation of volatile fragments from the surface of PDMS when the  
4  
5 siloxane component gets converted to silicon oxides during UVO treatment.<sup>36</sup>  
6  
7

8  
9 The variation in OFET characteristics for different annealing temperatures of Ph-BTBT-  
10  
11 10 can be correlated to the corresponding change in crystallinity and morphology of Ph-BTBT-10.  
12  
13 As the films were casted from a hot solution of Ph-BTBT-10 maintained at a temperature of  $\sim 110$   
14  
15  $^{\circ}\text{C}$  the un-annealed films showed the structural and morphological features of a SmE phase. The  
16  
17 SmE phase is characterized by the presence of a few number of monolayers and large number of  
18  
19 bilayer structures and this bilayer structure is preserved in the un-annealed film. The SmE phase  
20  
21 is known to exhibit closely packed herringbone structure, with a head to head orientation of two  
22  
23 molecules at the layer interface forming a bilayer, favoring two-dimensional charge conduction.<sup>9,</sup>  
24  
25  
26  
27 <sup>11, 53</sup> Hence, the OFET with un-annealed film exhibits good electrical characteristics. However,  
28  
29 when the film is annealed at  $120^{\circ}\text{C}$ , the number of bilayer structures in the sample has increased,  
30  
31 as observed from SAXS and AFM measurements, resulting in the exceptionally high performance  
32  
33 of corresponding OFETs. Conversely, as the annealing temperature is increased to  $180^{\circ}\text{C}$ , the  
34  
35 monolayer- bilayer intensities have equalized and the OFET performance degraded. A further  
36  
37 increase in annealing temperature to  $218^{\circ}\text{C}$  has resulted in a sudden drop in the OFET performance  
38  
39 due to the complete transition of the structure from bilayer to monolayer. Not only the structural  
40  
41 properties, but also the variation in grain size (as observed in the AFM images), and the  
42  
43 modification in the semiconductor- dielectric interface properties with annealing temperature  
44  
45 might have affected the performance of the OFETs. Moreover, the uniform alignment of LCs on  
46  
47 PDMS surface has contributed to the ease of charge transport through the LC semiconductor  
48  
49 channel. The PDMS surface might have acted as an alignment layer for the Ph-BTBT-10  
50  
51 molecules.<sup>54</sup>  
52  
53  
54  
55  
56  
57  
58  
59  
60

1  
2  
3 **Influence of Environmental conditions on OFET Performance.** The performance of organic  
4 devices are largely dependent on the environment in which it is operated. The fabrication and  
5 electrical characterization of the LC-OFETs discussed so far were carried out in ambient  
6 conditions. In order to observe its response in other environments, we have done the complete  
7 fabrication and electrical characterization of the OFET in nitrogen environment as well. Later, the  
8 OFET is taken to air and vacuum conditions. The characteristics obtained for the OFETs with Ph-  
9 BTBT-10 film annealed at 120 °C at different environments is as shown in figure 6 and the  
10 electrical parameters derived are given in table S5. The LC-OFET exhibited a very weak  
11 performance in nitrogen environment as compared to the superior performances observed in air as  
12 seen in the previous discussions, however non-idealities are not-present. The drain current became  
13 low and the off current is increased resulting in a low current on/ off ratio. The OFET showed  
14 positive threshold voltage as in a ‘normally on’ device. The performance of OFET is improved as  
15 it is taken into ambient environment (air) as seen in figure 6 (c, d). The mobility, current on/off  
16 ratio and threshold voltage showed noticeable enhancement in ambient conditions where the  
17 humidity is maintained at ~ 40%. However, the OFET performance is reduced when it is  
18 characterized in a vacuum ( $10^{-3}$  mbar) condition. Nonetheless, the current on/ off ratio was higher  
19 than that obtained when characterized in nitrogen atmosphere. The variation in OFET performance  
20 with environmental conditions can occur either due to the changes happening in the semiconductor  
21 or in the dielectric. Since we have adopted a BGTC configuration for OFET fabrication, the  
22 dielectric layer is placed beneath the semiconductor whereas, the semiconductor is directly  
23 exposed to outer environment. Moreover, PDMS is a highly hydrophobic and almost inert material  
24 to be effected by environmental changes. As a result, the observed change in electrical  
25 characteristics may be attributed to the direct interaction of Ph-BTBT-10 with the environment.  
26  
27  
28  
29  
30  
31  
32  
33  
34  
35  
36  
37  
38  
39  
40  
41  
42  
43  
44  
45  
46  
47  
48  
49  
50  
51  
52  
53  
54  
55  
56  
57  
58  
59  
60

Similar enhancement in hole conductivity is reported for polythiophene (P3HT) material when exposed to air.<sup>55</sup>

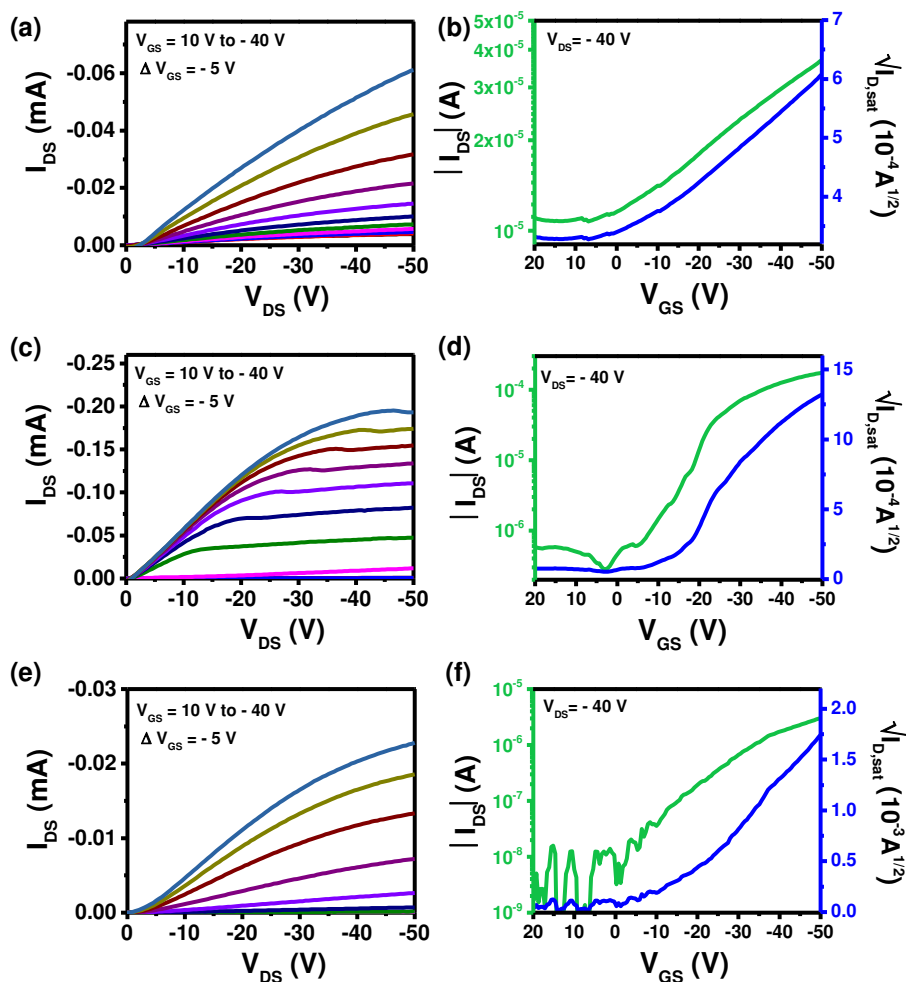
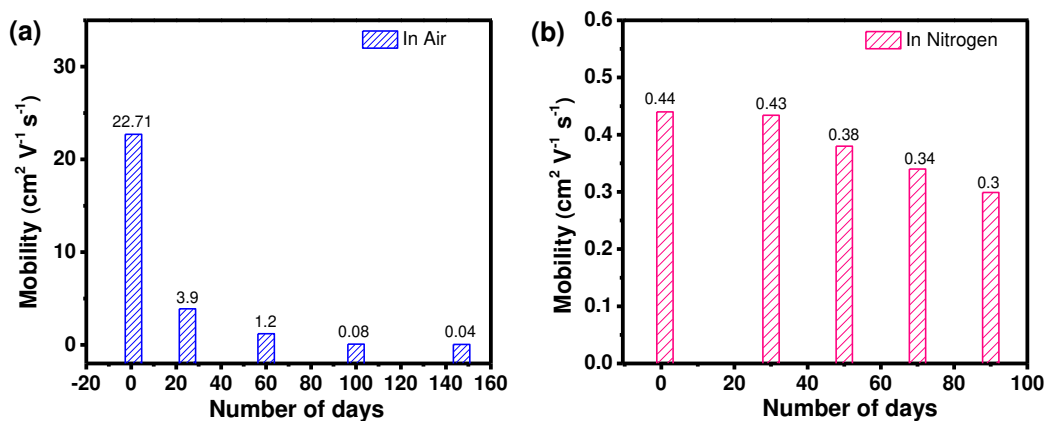


**Figure 6.** (a, c, e) Output characteristics ( $I_{DS}$ - $V_{DS}$ ) and (b, d, f) transfer characteristics ( $|I_{DS}|$ - $V_{GS}$  and  $\sqrt{|I_{D,sat}|}$ - $V_{GS}$ ) at  $V_{DS} = -40$  V of the OFET characterized in (a,b) nitrogen (c,d) air and (e,f) vacuum.

**Environmental stability of LC-OFETs.** The stability of the OFETs were analyzed by fabricating and storing the OFETs in air and nitrogen environments for more than three months. Even though

1  
2  
3 the OFET characterized in air exhibited high performance compared to the one characterized in  
4 nitrogen atmosphere, the device is found to be more stable in nitrogen than in ambient air. Figure  
5  
6  
7  
8  
9  
10  
11  
12  
13  
14  
15  
16  
17  
18  
19  
20  
21  
22  
23  
24  
25  
26  
27  
28  
29  
30  
31  
32  
33  
34  
35  
36  
37  
38  
39  
40  
41  
42  
43  
44  
45  
46  
47  
48  
49  
50  
51  
52  
53  
54  
55  
56  
57  
58  
59  
60

the OFET characterized in air exhibited high performance compared to the one characterized in nitrogen atmosphere, the device is found to be more stable in nitrogen than in ambient air. Figure 7 shows the variation in mobility of the OFETs with number of days of storage in air and nitrogen. The device stored in air shows a fast decay in mobility with storage time whereas the decay is slow in the device which is stored in nitrogen. The presence of air is responsible for an initial shoot-up in the mobility, however the storage in air causes a decay in performance due to the interaction of the organic components with water molecules and other impurities in air causing the creation of trap states and defects in the organic layers over time. The exact reason of enhanced performance and stability issue in air needs a detailed study which is beyond the scope of the present work.

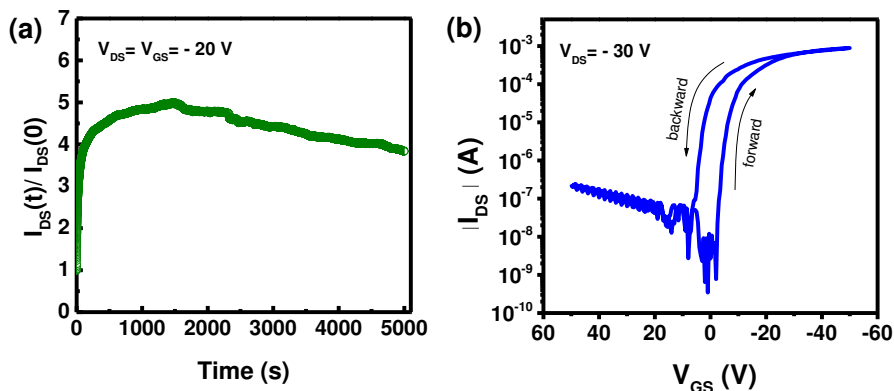


40  
41  
42  
43  
44  
45  
46  
47  
48  
49  
50  
51  
52  
53  
54  
55  
56  
57  
58  
59  
60

**Figure 7.** Variation in field effect mobility with number of days of storage (a) in air and (b) in nitrogen.

**Electrical Stability and hysteresis of PDMS based LC-OFETs.** The electrical stability of LC-OFET which is fabricated by annealing Ph-BTBT-10 layer at  $120^\circ\text{C}$  is studied by conducting bias-stress measurements in air. The drain and gate voltages (fixed at  $-20 \text{ V}$  each) were continuously applied for 5000 s and observed the variation in drain current with time. Unlike the exponential

1  
2  
3 decay normally observed in OFETs due to the presence of trap states, the LC-OFET in the present  
4 study exhibited anomalous current transients (figure 8a). Here, instead of a decay, the drain current  
5 showed an abrupt initial rise followed by a slow decay. The abrupt initial increase of  $I_{DS}$  can be  
6 mainly due to the slow-polarization of PDMS (due to its low dielectric constant). It can also occur  
7 due to the presence of dipolar groups on PDMS surface or due to the gate charge injection.<sup>56-57</sup> We  
8 also observed similar rise of current in nitrogen and vacuum also but the rate of increase is much  
9 smaller compared to that in air. Similarly, in humid conditions, a fast decay is observed which  
10 supports the fast decay in mobility shown by LC-OFET when stored in air. The fluctuations in  
11 ambient air and moisture show large influence on the LC-OFET performance. The bias-stress  
12 measurements indicate the high electrical stability of LC-OFETs against a continuous bias-stress.  
13  
14  
15  
16  
17  
18  
19  
20  
21  
22  
23  
24  
25  
26  
27  
28



29  
30  
31  
32  
33  
34  
35  
36  
37  
38  
39  
40  
41  
42  
43 **Figure 8.** (a) The normalized drain current versus time relation under the application of a  
44 continuous bias-stress ( $V_{DS} = V_{GS} = -20$  V) for 5000 s and (b) the transfer characteristics showing  
45 hysteresis for the LC-OFET with Ph-BTBT-10 layer annealed at  $120^{\circ}\text{C}$  when characterized in air.  
46  
47  
48  
49  
50  
51  
52

53 As shown in figure 8b, the LC-OFETs exhibit hysteresis behavior with a lower drain  
54 current during forward sweep (off to on) and a higher drain current during the backward sweep  
55  
56  
57  
58  
59  
60

1  
2  
3 (on to off). This kind of hysteresis can occur due to the same reasons that causes anomalous bias-  
4 stress behavior, which includes slow-polarization of PDMS and presence of polar functional  
5 groups on the gate dielectric.<sup>58</sup> As in the case of bias-stress, hysteresis is also found to be dependent  
6 on atmospheric conditions and is more pronounced in air than in nitrogen atmosphere. A detailed  
7 investigation on the bias-stress and hysteresis behavior of PDMS based OFETs and the role of  
8 semiconductors, atmospheric factors in it is being conducted. Suitable remedy for hysteresis nature  
9 is to be identified which may also reduce non-ideal behavior of the device.  
10  
11  
12  
13  
14  
15  
16  
17  
18  
19  
20  
21  
22

## 23 CONCLUSION

24  
25  
26 In summary, the high performance of LC-OFETs with the LC, Ph- BTBT-10 as channel material  
27 and the polymer elastomer, PDMS as gate dielectric is demonstrated. The devices exhibit high  
28 performances such as high hole mobility of  $\sim 22 \text{ cm}^2\text{V}^{-1}\text{s}^{-1}$ , low threshold voltage ( $< 1 \text{ V}$ ) and high  
29 current on/ off ratio of  $10^5$ , irrespective of the low dielectric constant of PDMS. The possibility of  
30 overestimation in mobility values due to the non-ideal transistor behavior was taken into account  
31 during mobility calculation. The annealing temperature of the LC is found to have large influence  
32 on the performance of the LC- OFETs. The OFET with Ph-BTBT-10 film annealed at  $120 \text{ }^\circ\text{C}$   
33 exhibits superior performance than the devices fabricated with un-annealed film and with the films  
34 annealed at  $180$  and  $218 \text{ }^\circ\text{C}$ . The enhanced performance is attributed to many factors like the  
35 bilayer structure and the large grain size of Ph-BTBT-10, and good dielectric-semiconductor  
36 interface properties. Moreover, the PDMS layer has acted as a proper alignment layer for the LC  
37 molecules, ensuring high carrier mobility for the OFETs through the channel. The LC-OFETs are  
38 found to be influenced by the environmental conditions in which it is operated, such as in air,  
39 nitrogen and vacuum conditions. The OFETs show anomalous bias-stress behavior and hysteresis,  
40  
41  
42  
43  
44  
45  
46  
47  
48  
49  
50  
51  
52  
53  
54  
55  
56  
57  
58  
59  
60

1  
2  
3 however, they are electrically stable. The transparent solution-processed LC-OFET is a promising  
4  
5 prototype for flexible electronics.  
6  
7  
8  
9  
10

## 11 ASSOCIATED CONTENT

12  
13  
14  
15 **Supporting Information.** (1) UVO treatment mechanism on PDMS surface, (2) primary  
16 characterization methods of Ph-BTBT-10: optical image of Ph-BTBT-10 thin-film, DSC curve,  
17 POM images of the phases of PhBTBT-10, (3) Capacitance- Frequency characteristics of PDMS,  
18 (4) table containing reliability factors of mobility, (5) table with average mobility of OFETs, (6)  
19 Mobility versus Annealing temperature plot, (7) Table containing the surface roughness of Ph-  
20 BTBT-10 thin-films, (8) AFM images of Ph-BTBT-10 on PDMS surface, (9) Table containing  
21 surface roughness of Ph-BTBT-10 thin-films on PDMS, (10) table containing electrical parameters  
22 of LC-OFET characterized at air, nitrogen and vacuum environments, (11) transfer characteristics  
23 showing hysteresis, (12) nature of hysteresis in air and nitrogen. (single PDF)  
24  
25  
26  
27  
28  
29  
30  
31  
32  
33  
34  
35  
36  
37  
38

## 39 AUTHOR INFORMATION

### 40 41 Corresponding Author

42  
43 **Manoj A. G. Namboothiry**

44  
45  
46  
47 School of Physics, Indian Institute of Science Education and Research- Thiruvananthapuram,  
48 Maruthamala P O, Vithura, Thiruvananthapuram, Kerala- 695551, India  
49

50  
51 ORCID: 0000-0002-7805-1962

52  
53 E-mail: [manoj@iisertvm.ac.in](mailto:manoj@iisertvm.ac.in)  
54  
55  
56  
57  
58  
59  
60

## Authors

### Reshma Raveendran

School of Physics, Indian Institute of Science Education and Research- Thiruvananthapuram,  
Maruthamala P O, Vithura, Thiruvananthapuram, Kerala- 695551, India

ORCID: 0000-0003-0866-3039

### Mamatha Nagaraj

School of Physics and Astronomy, University of Leeds, Leeds LS2 9JT, UK

ORCID: 0000-0001-9713-1362

E-mail: [m.nagaraj@leeds.ac.uk](mailto:m.nagaraj@leeds.ac.uk)

## Author Contributions

The manuscript was written through contributions of all authors. All authors have given approval to the final version of the manuscript.

## Notes

The authors declare no competing financial interest.

## ACKNOWLEDGMENTS

This work is supported by the Solar Energy Research Initiative (Department of Science and Technology, Government of India) and the Ministry of Human Resource and Development (Government of India). R.R. wishes to thank the Department of Science and Technology for the INSPIRE fellowship and the Newton- Bhabha short-term PhD placement program 2019 (jointly funded by British Council, UK and DST, India). M.A.G.N. and R.R. acknowledge Dr.

Ayyappanpillai Ajayaghosh and Dr. Bhoje E. Gowd, CSIR-National Institute for Interdisciplinary Science and Technology, Thiruvananthapuram for SAXS measurements.

## REFERENCES

- (1) Sirringhaus, H. 25th Anniversary Article: Organic Field-Effect Transistors: The Path Beyond Amorphous Silicon. *Advanced Materials* **2014**, *26* (9), 1319-1335, DOI: 10.1002/adma.201304346.
- (2) Yuan, Y.; Giri, G.; Ayzner, A. L.; Zoombelt, A. P.; Mannsfeld, S. C. B.; Chen, J.; Nordlund, D.; Toney, M. F.; Huang, J.; Bao, Z. Ultra-high mobility transparent organic thin film transistors grown by an off-centre spin-coating method. *Nature Communications* **2014**, *5* (1), 3005, DOI: 10.1038/ncomms4005.
- (3) Pei, K.; Wang, Z.; Ren, X.; Zhang, Z.; Peng, B.; Chan, P. K. L. Fully transparent organic transistors with junction-free metallic network electrodes. *Appl. Phys. Lett.* **2015**, *107* (3), 033302, DOI: 10.1063/1.4927445.
- (4) Lee, S.; Reuveny, A.; Reeder, J.; Lee, S.; Jin, H.; Liu, Q.; Yokota, T.; Sekitani, T.; Isoyama, T.; Abe, Y.; Suo, Z.; Someya, T. A transparent bending-insensitive pressure sensor. *Nature Nanotechnology* **2016**, *11* (5), 472-478, DOI: 10.1038/nnano.2015.324.
- (5) Liang, J.; Li, L.; Chen, D.; Hajagos, T.; Ren, Z.; Chou, S.-Y.; Hu, W.; Pei, Q. Intrinsically stretchable and transparent thin-film transistors based on printable silver nanowires, carbon nanotubes and an elastomeric dielectric. *Nature Communications* **2015**, *6* (1), 7647, DOI: 10.1038/ncomms8647.
- (6) Halik, M.; Klauk, H.; Zschieschang, U.; Schmid, G.; Radlik, W.; Weber, W. Polymer Gate Dielectrics and Conducting-Polymer Contacts for High-Performance Organic Thin-Film Transistors. *Advanced Materials* **2002**, *14* (23), 1717-1722, DOI: 10.1002/1521-4095(20021203)14:23<1717::aid-adma1717>3.0.co;2-g.
- (7) Veres, J.; Ogier, S.; Lloyd, G.; de Leeuw, D. Gate Insulators in Organic Field-Effect Transistors. *Chemistry of Materials* **2004**, *16* (23), 4543-4555, DOI: 10.1021/cm049598q.
- (8) Nketia-Yawson, B.; Noh, Y.-Y. Recent Progress on High-Capacitance Polymer Gate Dielectrics for Flexible Low-Voltage Transistors. *Advanced Functional Materials* **2018**, *28* (42), 1802201, DOI: 10.1002/adfm.201802201.
- (9) Iino, H.; Usui, T.; Hanna, J.-i. Liquid crystals for organic thin-film transistors. *Nature Communications* **2015**, *6* (1), 6828, DOI: 10.1038/ncomms7828.
- (10) Kunii, M.; Iino, H.; Hanna, J. Solution-Processed, Low-Voltage Polycrystalline Organic Field-Effect Transistor Fabricated Using Highly Ordered Liquid Crystal With Low- $\epsilon$  Gate Dielectric. *IEEE Electron Device Letters* **2016**, *37* (4), 486-488, DOI: 10.1109/LED.2016.2529678.
- (11) Kim, S.; Kim, A.; Jang, K.-S.; Yoo, S.; Ka, J.-W.; Kim, J.; Yi, M. H.; Won, J. C.; Hong, S.-K.; Kim, Y. H. The effect of thermal annealing on the layered structure of smectic liquid crystalline organic semiconductor on polyimide gate insulator and its OFET performance. *Synthetic Metals* **2016**, *220*, 311-317, DOI: <https://doi.org/10.1016/j.synthmet.2016.06.021>.

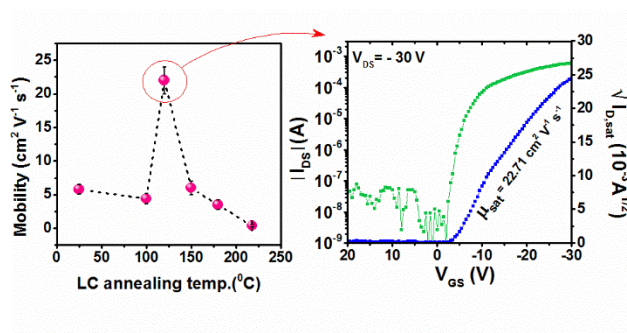
- 1  
2  
3 (12) Wang, Y.; Huang, X.; Li, T.; Li, L.; Guo, X.; Jiang, P. Polymer-Based Gate Dielectrics for  
4 Organic Field-Effect Transistors. *Chemistry of Materials* **2019**, *31* (7), 2212-2240, DOI:  
5 10.1021/acs.chemmater.8b03904.  
6  
7 (13) He, D.; Qiao, J.; Zhang, L.; Wang, J.; Lan, T.; Qian, J.; Li, Y.; Shi, Y.; Chai, Y.; Lan, W.;  
8 Ono, L. K.; Qi, Y.; Xu, J.-B.; Ji, W.; Wang, X. Ultrahigh mobility and efficient charge injection  
9 in monolayer organic thin-film transistors on boron nitride. *Science Advances* **2017**, *3* (9),  
10 e1701186, DOI: 10.1126/sciadv.1701186.  
11 (14) Lee, J.; Kang, S.-H.; Lee, S. M.; Lee, K. C.; Yang, H.; Cho, Y.; Han, D.; Li, Y.; Lee, B. H.;  
12 Yang, C. An Ultrahigh Mobility in Isomorphous Fluorobenzo[c][1,2,5]thiadiazole-Based  
13 Polymers. *Angewandte Chemie International Edition* **2018**, *57* (41), 13629-13634, DOI:  
14 10.1002/anie.201808098.  
15 (15) Lee, B. H.; Hsu, B. B. Y.; Patel, S. N.; Labram, J.; Luo, C.; Bazan, G. C.; Heeger, A. J.  
16 Flexible Organic Transistors with Controlled Nanomorphology. *Nano Letters* **2016**, *16* (1), 314-  
17 319, DOI: 10.1021/acs.nanolett.5b03868.  
18 (16) Li, J.; Zhao, Y.; Tan, H. S.; Guo, Y.; Di, C.-A.; Yu, G.; Liu, Y.; Lin, M.; Lim, S. H.; Zhou,  
19 Y.; Su, H.; Ong, B. S. A stable solution-processed polymer semiconductor with record high-  
20 mobility for printed transistors. *Scientific Reports* **2012**, *2* (1), 754, DOI: 10.1038/srep00754.  
21 (17) Tseng, H.-R.; Phan, H.; Luo, C.; Wang, M.; Perez, L. A.; Patel, S. N.; Ying, L.; Kramer, E.  
22 J.; Nguyen, T.-Q.; Bazan, G. C.; Heeger, A. J. High-Mobility Field-Effect Transistors Fabricated  
23 with Macroscopic Aligned Semiconducting Polymers. *Advanced Materials* **2014**, *26* (19), 2993-  
24 2998, DOI: 10.1002/adma.201305084.  
25 (18) Wang, Q.; Jiang, S.; Qian, J.; Song, L.; Zhang, L.; Zhang, Y.; Zhang, Y.; Wang, Y.; Wang,  
26 X.; Shi, Y.; Zheng, Y.; Li, Y. Low-voltage, High-performance Organic Field-Effect Transistors  
27 Based on 2D Crystalline Molecular Semiconductors. *Scientific Reports* **2017**, *7* (1), 7830, DOI:  
28 10.1038/s41598-017-08280-8.  
29 (19) Xu, X.; Yao, Y.; Shan, B.; Gu, X.; Liu, D.; Liu, J.; Xu, J.; Zhao, N.; Hu, W.; Miao, Q.  
30 Electron Mobility Exceeding  $10 \text{ cm}^2 \text{ V}^{-1} \text{ s}^{-1}$  and Band-Like Charge Transport in Solution-  
31 Processed n-Channel Organic Thin-Film Transistors. *Advanced Materials* **2016**, *28* (26), 5276-  
32 5283, DOI: 10.1002/adma.201601171.  
33 (20) Piliego, C.; Jarzab, D.; Gigli, G.; Chen, Z.; Facchetti, A.; Loi, M. A. High Electron Mobility  
34 and Ambient Stability in Solution-Processed Perylene-Based Organic Field-Effect Transistors.  
35 *Advanced Materials* **2009**, *21* (16), 1573-1576, DOI: 10.1002/adma.200803207.  
36 (21) Tang, W.; Feng, L.; Yu, P.; Zhao, J.; Guo, X. Highly Efficient All-Solution-Processed Low-  
37 Voltage Organic Transistor with a Micrometer-Thick Low-k Polymer Gate Dielectric Layer.  
38 *Advanced Electronic Materials* **2016**, *2* (5), 1500454, DOI: 10.1002/aelm.201500454.  
39 (22) Zhao, J.; Tang, W.; Li, Q.; Liu, W.; Guo, X. Fully Solution Processed Bottom-Gate Organic  
40 Field-Effect Transistor With Steep Subthreshold Swing Approaching the Theoretical Limit.  
41 *IEEE Electron Device Letters* **2017**, *38* (10), 1465-1468.  
42 (23) Shin, E.-Y.; Choi, E.-Y.; Noh, Y.-Y. Parylene based bilayer flexible gate dielectric layer for  
43 top-gated organic field-effect transistors. *Organic Electronics* **2017**, *46*, 14-21, DOI:  
44 <https://doi.org/10.1016/j.orgel.2017.04.005>.  
45 (24) Wang, B.; Huang, W.; Chi, L.; Al-Hashimi, M.; Marks, T. J.; Facchetti, A. High-k Gate  
46 Dielectrics for Emerging Flexible and Stretchable Electronics. *Chem. Rev.* **2018**, *118* (11), 5690-  
47 5754, DOI: 10.1021/acs.chemrev.8b00045.  
48  
49  
50  
51  
52  
53  
54  
55  
56  
57  
58  
59  
60

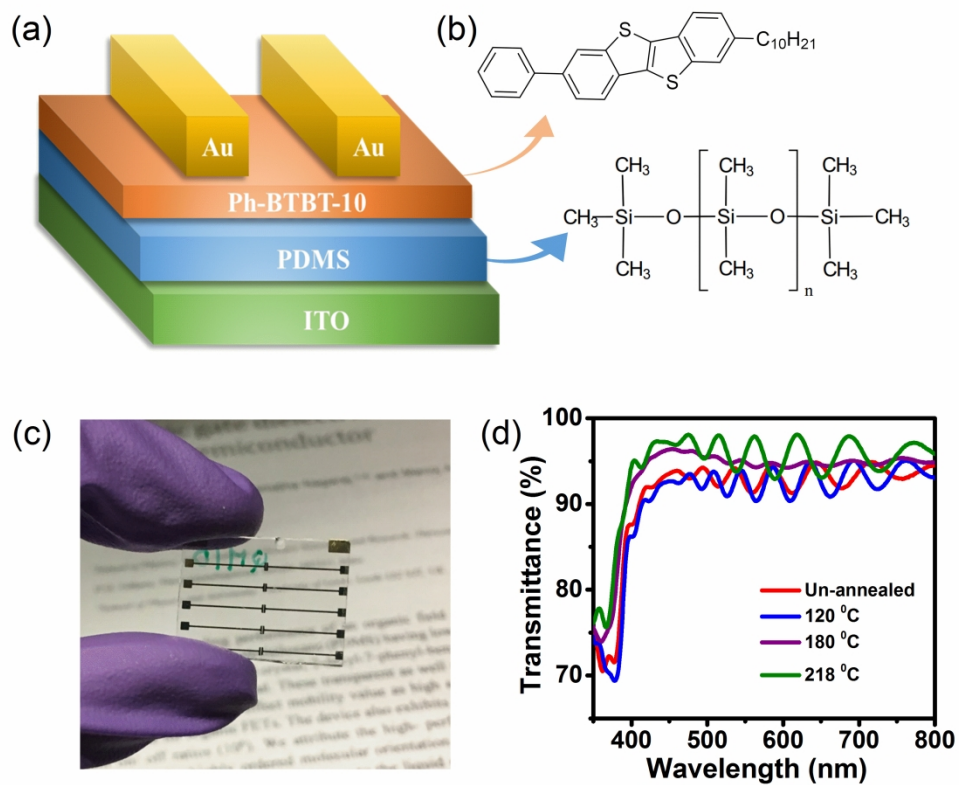
- 1  
2  
3 (25) Park, H.; Yoo, S.; Yi, M. H.; Kim, Y. H.; Jung, S. Flexible and stable organic field-effect  
4 transistors using low-temperature solution-processed polyimide gate dielectrics. *Organic*  
5 *Electronics* **2019**, *68*, 70-75, DOI: <https://doi.org/10.1016/j.orgel.2019.01.043>.  
6  
7 (26) Facchetti, A.; Yoon, M.-H.; Marks, T. J. Gate Dielectrics for Organic Field-Effect  
8 Transistors: New Opportunities for Organic Electronics. *Advanced Materials* **2005**, *17* (14),  
9 1705-1725, DOI: 10.1002/adma.200500517.  
10  
11 (27) Veres, J.; Ogier, S. D.; Leeming, S. W.; Cupertino, D. C.; Mohialdin Khaffaf, S. Low-k  
12 Insulators as the Choice of Dielectrics in Organic Field-Effect Transistors. *Advanced Functional*  
13 *Materials* **2003**, *13* (3), 199-204, DOI: 10.1002/adfm.200390030.  
14  
15 (28) Lee, J.; Chung, J. W.; Yoon, G. B.; Lee, M. H.; Kim, D. H.; Park, J.; Lee, J.-K.; Kang, M. S.  
16 Influence of Dielectric Layers on Charge Transport through Diketopyrrolopyrrole-Containing  
17 Polymer Films: Dielectric Polarizability vs Capacitance. *ACS Applied Materials & Interfaces*  
18 **2016**, *8* (44), 30344-30350, DOI: 10.1021/acsami.6b09993.  
19  
20 (29) Lee, S.-H.; Xu, Y.; Khim, D.; Park, W.-T.; Kim, D.-Y.; Noh, Y.-Y. Effect of Polymer Gate  
21 Dielectrics on Charge Transport in Carbon Nanotube Network Transistors: Low-k Insulator for  
22 Favorable Active Interface. *ACS Applied Materials & Interfaces* **2016**, *8* (47), 32421-32431,  
23 DOI: 10.1021/acsami.6b06882.  
24  
25 (30) Reese, C.; Chung, W.-J.; Ling, M.-m.; Roberts, M.; Bao, Z. High-performance microscale  
26 single-crystal transistors by lithography on an elastomer dielectric. *Appl. Phys. Lett.* **2006**, *89*  
27 (20), 202108, DOI: 10.1063/1.2388151.  
28  
29 (31) Graz, I. M.; Lacour, S. P. Flexible pentacene organic thin film transistor circuits fabricated  
30 directly onto elastic silicone membranes. *Appl. Phys. Lett.* **2009**, *95* (24), 243305, DOI:  
31 10.1063/1.3265737.  
32  
33 (32) Orgiu, E.; Manunza, I.; Sanna, M.; Cosseddu, P.; Bonfiglio, A. Transparent dielectric films  
34 for organic thin-film transistors: A perspective for low cost, low size technologies. *Thin Solid*  
35 *Films* **2008**, *516* (7), 1533-1537, DOI: <https://doi.org/10.1016/j.tsf.2007.03.157>.  
36  
37 (33) Zhou, S.; Li, M.; Tang, Q.; Song, Z.; Tong, Y.; Liu, Y. Deposition of Pentacene Thin Film  
38 on Polydimethylsiloxane Elastic Dielectric Layer for Flexible Thin-Film Transistors. *IEEE*  
39 *Electron Device Letters* **2017**, *38* (8), 1031-1034.  
40  
41 (34) McDonald, J. C.; Whitesides, G. M. Poly(dimethylsiloxane) as a Material for Fabricating  
42 Microfluidic Devices. *Acc. Chem. Res.* **2002**, *35* (7), 491-499, DOI: 10.1021/ar010110q.  
43  
44 (35) Law, K.-Y.; Zhao, H. *Surface wetting: characterization, contact angle, and fundamentals*,  
45 Springer 2015.  
46  
47 (36) Raveendran, R.; Namboothiry, M. A. G. Surface-Treated Poly(dimethylsiloxane) as a Gate  
48 Dielectric in Solution-Processed Organic Field-Effect Transistors. *ACS Omega* **2018**, *3* (9),  
49 11278-11285, DOI: 10.1021/acsomega.8b01629.  
50  
51 (37) Yamamura, A.; Sakon, T.; Takahira, K.; Wakimoto, T.; Sasaki, M.; Okamoto, T.;  
52 Watanabe, S.; Takeya, J. High-Speed Organic Single-Crystal Transistor Responding to Very  
53 High Frequency Band. *Advanced Functional Materials* **2020**, *30* (11), 1909501, DOI:  
54 10.1002/adfm.201909501.  
55  
56 (38) Guo, X.; Balon, F.; Hatton, R. A.; Shannon, J. M. In *High Performance Transistors in Low*  
57 *Mobility Organic Semiconductors for Analog and High-Frequency Applications*, 2008 Flexible  
58 Electronics and Displays Conference and Exhibition, 21-24 Jan. 2008; 2008; pp 1-5.  
59  
60 (39) Quinn, J. T. E.; Zhu, J.; Li, X.; Wang, J.; Li, Y. Recent progress in the development of n-  
type organic semiconductors for organic field effect transistors. *Journal of Materials Chemistry*  
*C* **2017**, *5* (34), 8654-8681, DOI: 10.1039/C7TC01680H.

- (40) McCulloch, I.; Heeney, M.; Bailey, C.; Genevicius, K.; MacDonald, I.; Shkunov, M.; Sparrowe, D.; Tierney, S.; Wagner, R.; Zhang, W.; Chabinyk, M. L.; Kline, R. J.; McGehee, M. D.; Toney, M. F. Liquid-crystalline semiconducting polymers with high charge-carrier mobility. *Nature Materials* **2006**, *5* (4), 328-333, DOI: 10.1038/nmat1612.
- (41) Funahashi, M. Development of Liquid-Crystalline Semiconductors with High Carrier Mobilities and Their Application to Thin-film Transistors. *Polymer Journal* **2009**, *41* (6), 459-469, DOI: 10.1295/polymj.PJ2008324.
- (42) Choi, H. H.; Cho, K.; Frisbie, C. D.; Sirringhaus, H.; Podzorov, V. Critical assessment of charge mobility extraction in FETs. *Nature Materials* **2018**, *17* (1), 2-7, DOI: 10.1038/nmat5035.
- (43) Gundlach, D. J.; Zhou, L.; Nichols, J. A.; Jackson, T. N.; Necliudov, P. V.; Shur, M. S. An experimental study of contact effects in organic thin film transistors. *J. Appl. Phys.* **2006**, *100* (2), 024509, DOI: 10.1063/1.2215132.
- (44) Phan, H.; Ford, M. J.; Lill, A. T.; Wang, M.; Bazan, G. C.; Nguyen, T.-Q. Electrical Double-Slope Nonideality in Organic Field-Effect Transistors. *Advanced Functional Materials* **2018**, *28* (17), 1707221, DOI: 10.1002/adfm.201707221.
- (45) Park, S.; Lee, B.; Bae, B.; Chai, J.; Lee, S.; Kim, C. Ambipolar thin-film transistors based on organic semiconductor blend. *Synthetic Metals* **2019**, *253*, 40-47, DOI: <https://doi.org/10.1016/j.synthmet.2019.05.001>.
- (46) Bittle, E. G.; Basham, J. I.; Jackson, T. N.; Jurchescu, O. D.; Gundlach, D. J. Mobility overestimation due to gated contacts in organic field-effect transistors. *Nature Communications* **2016**, *7* (1), 10908, DOI: 10.1038/ncomms10908.
- (47) Paterson, A. F.; Singh, S.; Fallon, K. J.; Hodsdon, T.; Han, Y.; Schroeder, B. C.; Bronstein, H.; Heeney, M.; McCulloch, I.; Anthopoulos, T. D. Recent Progress in High-Mobility Organic Transistors: A Reality Check. *Advanced Materials* **2018**, *30* (36), 1801079, DOI: 10.1002/adma.201801079.
- (48) Un, H.-I.; Wang, J.-Y.; Pei, J. Recent Efforts in Understanding and Improving the Nonideal Behaviors of Organic Field-Effect Transistors. *Advanced Science* **2019**, *6* (20), 1900375, DOI: 10.1002/advs.201900375.
- (49) Liu, M.; Sun, J.; Chen, Q. Influences of heating temperature on mechanical properties of polydimethylsiloxane. *Sensors and Actuators A: Physical* **2009**, *151* (1), 42-45, DOI: <https://doi.org/10.1016/j.sna.2009.02.016>.
- (50) Inoue, S.; Minemawari, H.; Tsutsumi, J. y.; Chikamatsu, M.; Yamada, T.; Horiuchi, S.; Tanaka, M.; Kumai, R.; Yoneya, M.; Hasegawa, T. Effects of Substituted Alkyl Chain Length on Solution-Processable Layered Organic Semiconductor Crystals. *Chemistry of Materials* **2015**, *27* (11), 3809-3812, DOI: 10.1021/acs.chemmater.5b00810.
- (51) Iino, H.; Hanna, J.-I. Liquid crystal and crystal structures of a phenyl-benzothienobenzothiophene derivative. *Mol. Cryst. Liq. Cryst.* **2017**, *647* (1), 37-43, DOI: 10.1080/15421406.2017.1289427.
- (52) Cullity, B. D. Elements of X-ray diffraction, Addison. *Wesley Mass* **1978**.
- (53) Minemawari, H.; Tsutsumi, J. y.; Inoue, S.; Yamada, T.; Kumai, R.; Hasegawa, T. Crystal structure of asymmetric organic semiconductor 7-decyl-2-phenyl[1]benzothieno[3,2-b][1]benzothiophene. *Applied Physics Express* **2014**, *7* (9), 091601, DOI: 10.7567/apex.7.091601.
- (54) Sun, X.; Di, C.-a.; Liu, Y. Engineering of the dielectric-semiconductor interface in organic field-effect transistors. *Journal of Materials Chemistry* **2010**, *20* (13), 2599-2611, DOI: 10.1039/B921449F.

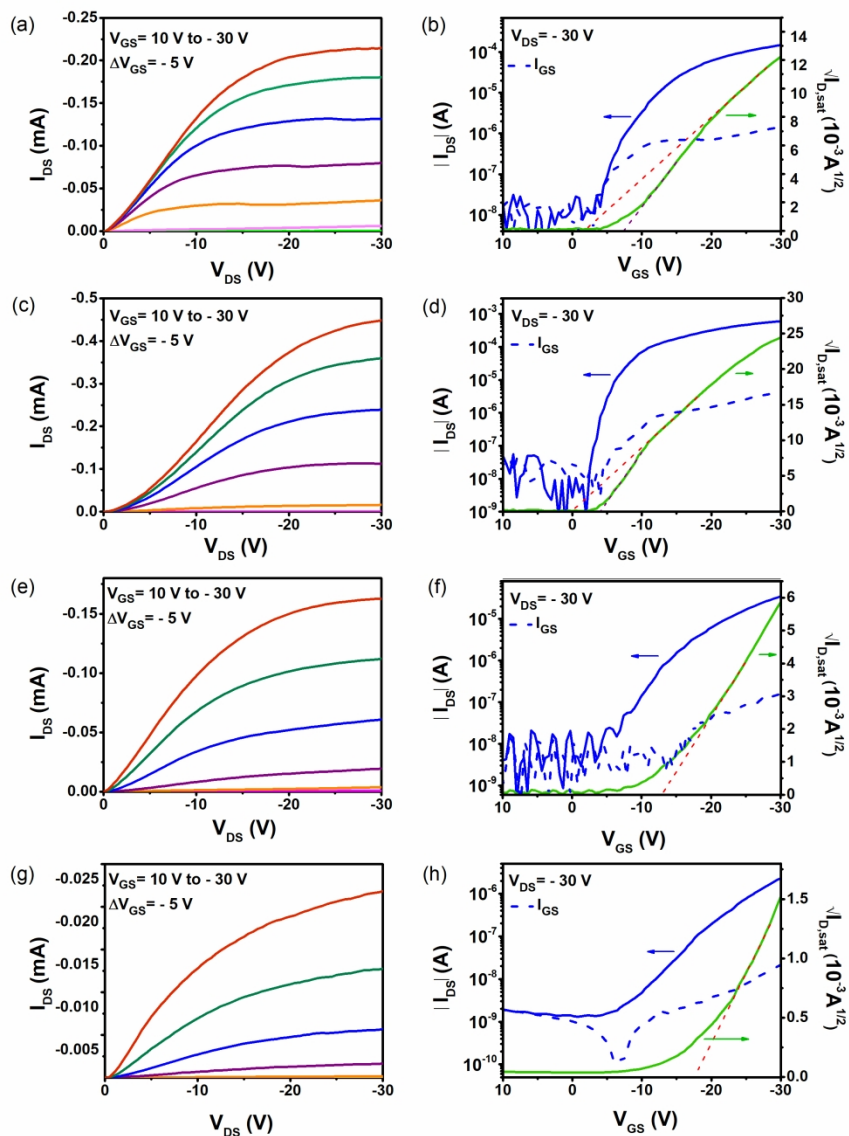
- 1  
2  
3 (55) Abdou, M. S. A.; Orfino, F. P.; Son, Y.; Holdcroft, S. Interaction of Oxygen with  
4 Conjugated Polymers: Charge Transfer Complex Formation with Poly(3-alkylthiophenes). *J.*  
5 *Am. Chem. Soc.* **1997**, *119* (19), 4518-4524, DOI: 10.1021/ja964229j.  
6  
7 (56) Kim, J.; Jang, J.; Kim, K.; Kim, H.; Kim, S. H.; Park, C. E. The Origin of Excellent Gate-  
8 Bias Stress Stability in Organic Field-Effect Transistors Employing Fluorinated-Polymer Gate  
9 Dielectrics. *Advanced Materials* **2014**, *26* (42), 7241-7246, DOI: 10.1002/adma.201402363.  
10  
11 (57) de Pauli, M.; Zschieschang, U.; Barcelos, I. D.; Klauk, H.; Malachias, A. Tailoring the  
12 Dielectric Layer Structure for Enhanced Carrier Mobility in Organic Transistors: The Use of  
13 Hybrid Inorganic/Organic Multilayer Dielectrics. *Advanced Electronic Materials* **2016**, *2* (5),  
14 1500402, DOI: 10.1002/aelm.201500402.  
15  
16 (58) Egginger, M.; Bauer, S.; Schwödiauer, R.; Neugebauer, H.; Sariciftci, N. S. Current versus  
17 gate voltage hysteresis in organic field effect transistors. *Monatsh. Chem.* **2009**, *140*, 735-750,  
18 DOI: 10.1007/s00706-009-0149-z.  
19  
20  
21  
22  
23  
24  
25  
26  
27  
28  
29  
30  
31  
32  
33  
34  
35  
36  
37  
38  
39  
40  
41  
42  
43  
44  
45  
46  
47  
48  
49  
50  
51  
52  
53  
54  
55  
56  
57  
58  
59  
60

For Table of Contents Only

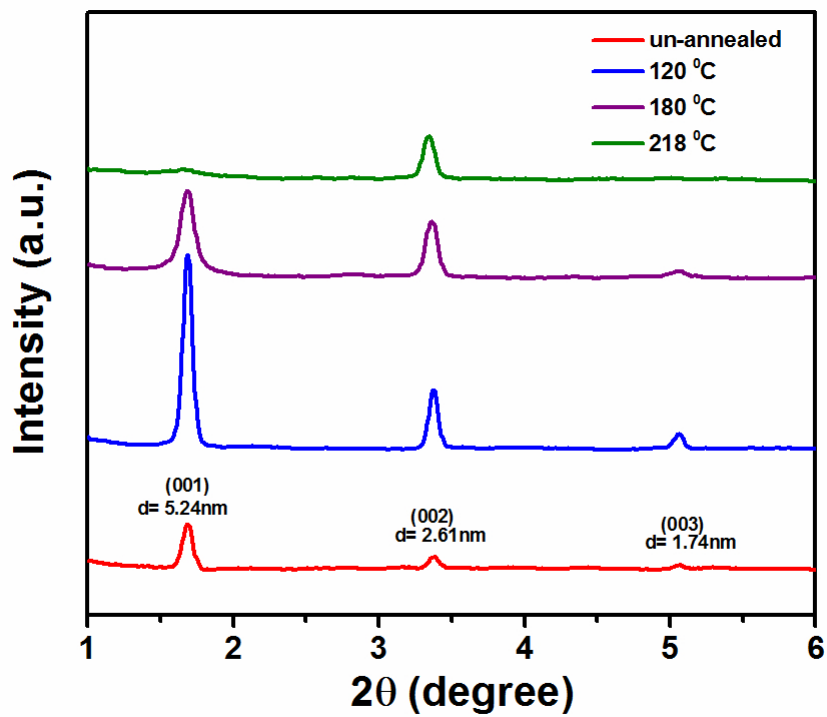




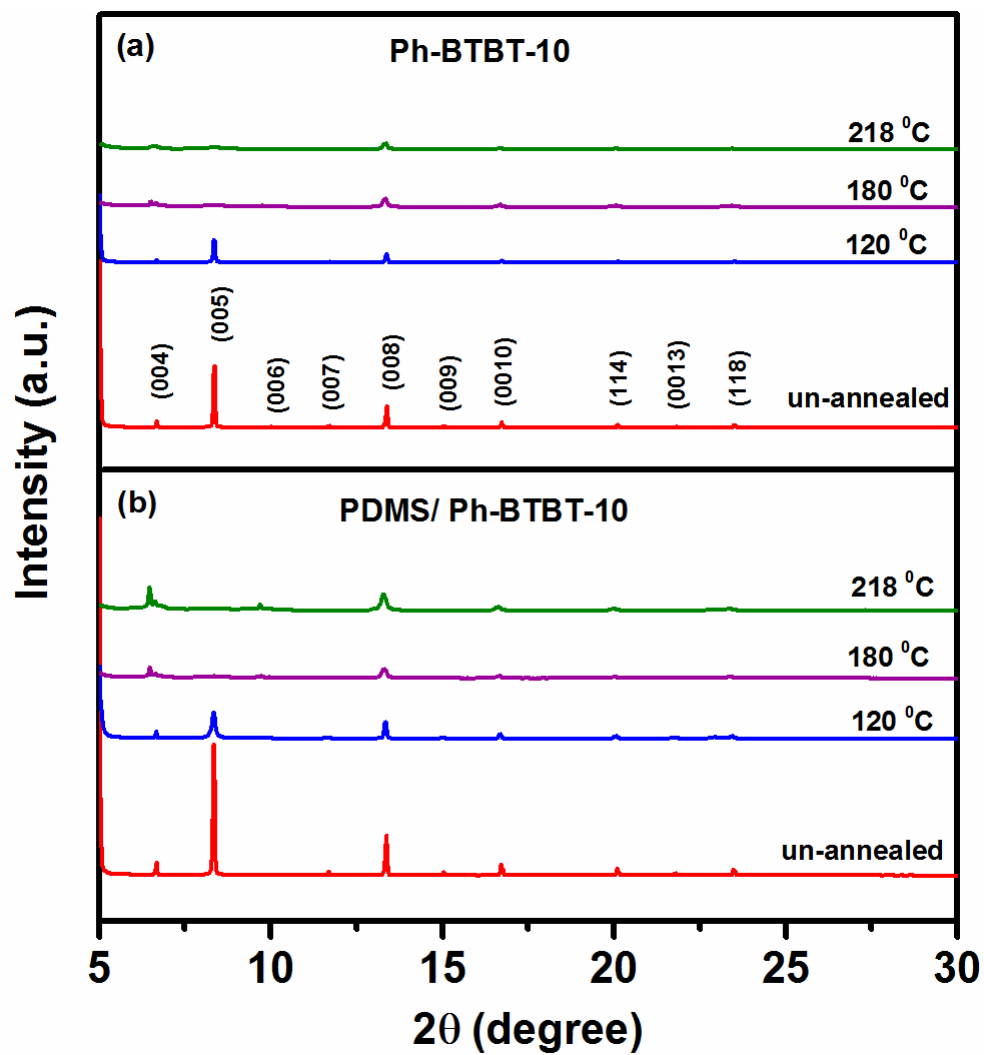
152x131mm (600 x 600 DPI)



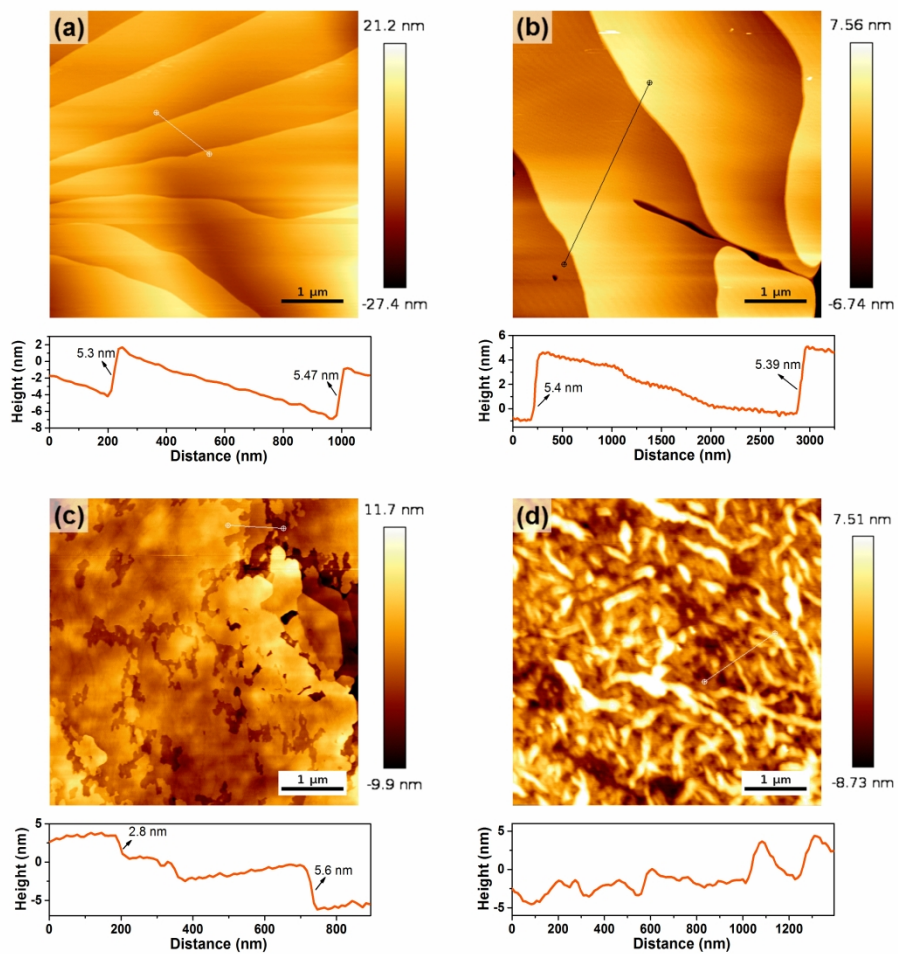
211x295mm (300 x 300 DPI)



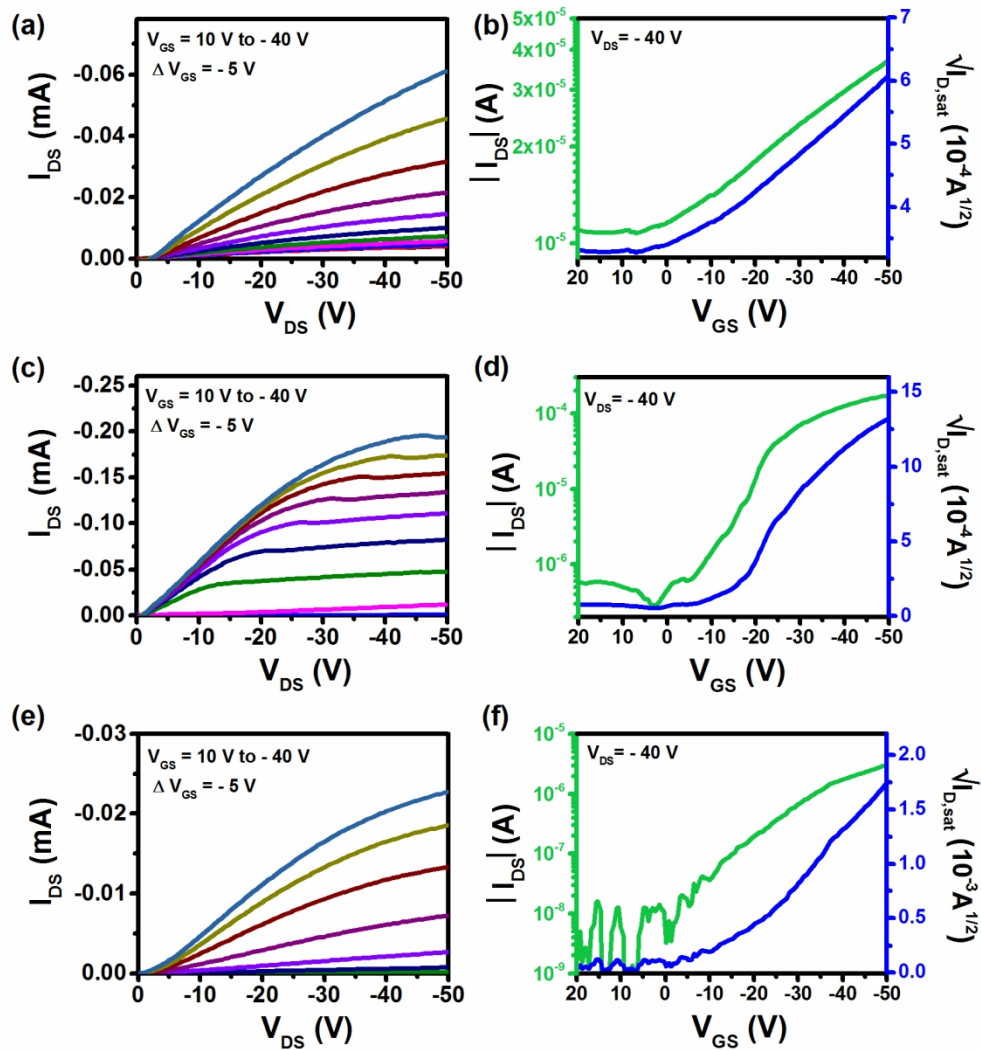
84x64mm (300 x 300 DPI)



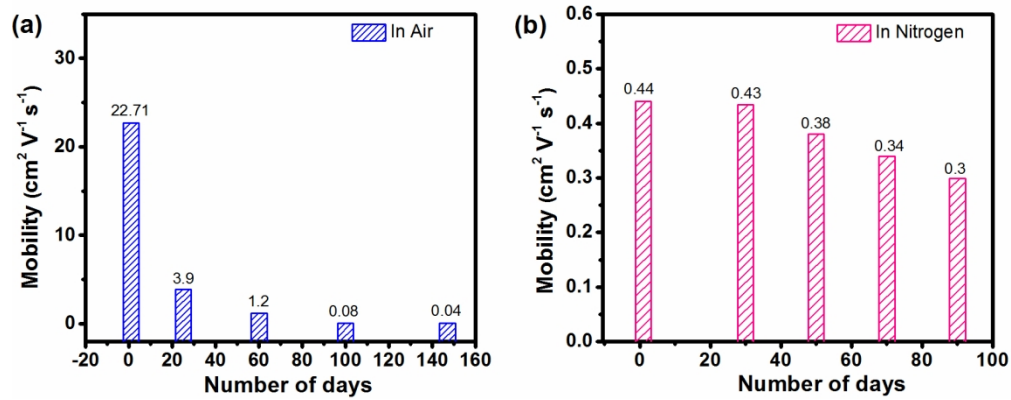
84x90mm (300 x 300 DPI)



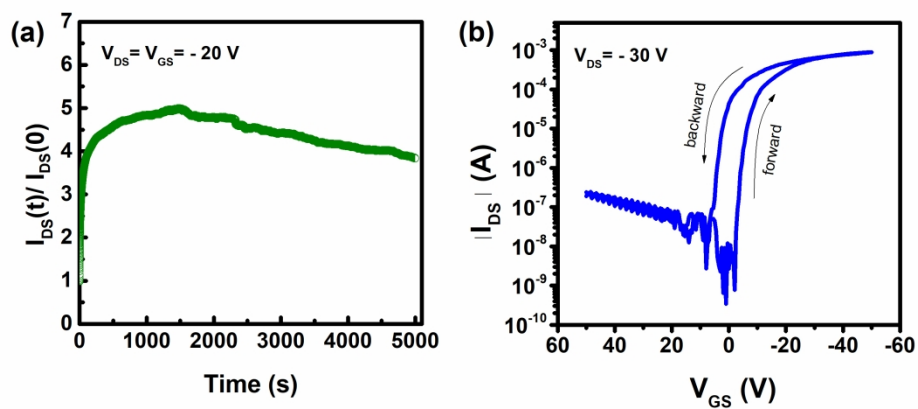
177x176mm (600 x 600 DPI)



152x169mm (300 x 300 DPI)



152x61mm (300 x 300 DPI)



273x122mm (300 x 300 DPI)